UNIVERSITY OF CALIFORNIA, SAN DIEGO

3D Photopatterning of Hydrogels with Applications in Cancer Growth Models

A Thesis submitted in partial satisfaction of the requirements
for the degree Master of Science

in

Bioengineering

by

Shruti Krishna Davey

Committee in charge:

Professor Shyni Varghese, Chair
Professor Gaurav Arya
Professor Christian Metallo

2016

The Thesis of Shruti Krishna Davey is approved and it is acceptable in quality and form for publication on microfilm and electronically:

Chair

University of California, San Diego

2016

TABLE OF CONTENTS

LIST OF FIGURES

ACKNOWLEDGEMENTS

My deepest gratitude goes to all of my family, who have always been very supportive of my endeavors, and who have guided me through my successes and my struggles. Specifically, I would like to acknowledge my parents, Uma and Krishna who have given their constant support and love, and have patiently encouraged me to be a strong and determined individual. I would like thank the one person who will forever be one of my best friends, my little sister Smriti. She is the joy in my life, and I truly appreciate her for teaching me responsibility and demonstrating selflessness and compassion to everyone. I would also like to thank my husband, Hari, for being there for me, especially when I needed encouragement during my graduate school experience. Next, I would like to thank my grandparents, Saraswati and Sundaresha, for believing in me, and constantly saying "KG to PG, first-class first, gold medalist!"

I would like to acknowledge my advisor, Professor Shyni Varghese, for accepting me into her lab and giving me the opportunity to work with her. She has patiently guided me through these years, and has also helped me recognize my strengths and weaknesses to better prepare me for my professional career. I deeply appreciate her taking all that time to talk to me and help me with my research. I would also like to thank Professors Gaurav Arya and Christian Metallo for agreeing to be a part of my committee, and I appreciate all their feedback in making this thesis possible.

Lastly, I would like to thank my lab members for their constant encouragement and support. Particularly, my graduate experience was strongly shaped by Aereas Aung. His never-ending excitement about science and research was a strong motivating factor. His creative thinking was always an inspiration to me. I want to thank him for helping

me with my research, and also for just being a good listener and answering all my questions and concerns.

Chapter 2, in full, is a reformatted reprint of the material as it appears in Tissue Engineering Part C Methods, Nov; 21(11):1188-96, 2015. "Embedded 3D photo-patterning of hydrogels with diverse and complex architectures for tissue engineering and disease models." Davey, Shruti Krishna*; Aung, Aereas*; Agrawal, Gaurav; Lim, Han Liang; Kar, Mrityunjoy; and Varghese, Shyni. The thesis author was a primary investigator and author of this paper.

The authors acknowledge Jomkuan Theprungsirikul for her assistance with taking the photographs. Research reported in this publication was supported by the National Institute of Arthritis and Musculoskeletal and Skin Diseases of the National Institutes of Health under Award Number R01 AR063184-02 and the California Institute of Regenerative Medicine (grant RT3-07907). Aereas Aung would like to acknowledge the support from Ruth L. Kirschstein National Research Service Award NIH/NHLBI T32 HL 105373, and ARCS Foundation. The authors also acknowledge the University of California San Diego Neuroscience Microscopy Shared Facility funded through NS047101. The hMSCs used in this study were provided by the Institute for Regenerative Medicine, Texas A&M University, through Grant P40RR017447 from the National Center for Research Resources (NCRR) of the NIH.

Chapter 3, in full, is a result of collaborative work with Aereas Aung. The author also acknowledges Professor Juan Carlos del Alamo and his research group for the Particle Image Velocimetry MATLAB algorithm. Finally, the author acknowledges Jomkuan Theprungsirikul for guidance in microfluidics device preparation and help

with cell encapsulation steps. The thesis author was a primary investigator and author of this chapter.

ABSTRACT OF THE THESIS

3D Photopatterning of Hydrogels with Applications in Cancer Growth Models

by

Shruti Krishna Davey

Master of Science in Bioengineering

University of California, San Diego, 2016

Professor Shyni Varghese, Chair

Techniques for cellular encapsulation within three-dimensional (3D) structures, such as bioprinting and patterning methods, play an important role in creating complex and hierarchically organized tissues, as well as when studying cell-cell and cell-matrix interactions. To this end, advances in technologies have enabled development of

methods to generate such 3D structures. We describe an easy-to-use photopatterning method involving photomask and a simple fluorescence microscope. This method is adapted to generate homogeneous and co-culture tissue constructs. Additionally, we extend this approach to establish a system to quantitatively study cancer spheroid growth. We developed a method combining the photomask-based 3D photopatterning technique with microfluidics technology to encapsulate a cancer spheroid within a patterned hydrogel embedded with fluorescent particles, monitor the cancer growth, and quantify the corresponding relative changes in the mechanical properties of the surrounding extracellular matrix (ECM). In this method, we applied hydrostatic pressure to compress the acellular and cell-laden gelatin methacrylate (GelMA) structure to detect volumetric strains. In the case of cell-laden GelMA hydrogel, we applied hydrostatic pressure at different culture timepoints, and recorded the changes in the local volumetric strains and compared it to a finite element simulation. We assess the possibility of this approach to deduce the approximate changes in the material properties during the cancer spheroid growth.

CHAPTER 1: INTRODUCTION

1.1 Background

In recent years, there has been increasing evidence of the physiological relevance of tissue organization and interactions within tissues, particularly cell-cell and cell-extracellular matrix (cell-ECM) interactions, and the overall importance of the microenvironment (1–3). The microenvironment, consisting of extracellular matrix proteins, growth factors, and stromal cells, dynamically influence the cells and therefore, the overall function is well regulated (1–5). Thus, when tissue constructs are generated for implantation purposes, or when in vitro systems are designed to study physiological conditions or disease states, there has been growing evidence for the need to shift from two-dimensional (2D) to three-dimensional (3D) systems to better mimic the natural environment (1,6). This shift towards 3D culture systems started in the field of tissue engineering, starting with studies of scaffolds and hydrogels to function as the substrates for in vitro cell survival, growth and differentiation, behaviors in accordance with their normal physiological states (1,7,8).

More recently, these 3D culture strategies have been imbibed in studies of disease states, particularly cancer, with the recognition that the interactions between cancer cells and their 3D microenvironment have strong influence in cancer progression (6,8). Statistics showing that more than 1.6 million new cases of cancer were projected for the year 2016 in the United States alone and that globally there were approximately 14.1 million new diagnoses for the year 2012 indicate the high prevalence of the disease

worldwide, and the importance of cancer research for providing insights into development of treatments and cures (9,10). Further, significant efforts have been put into increasing the complexities of the in vitro 3D culture systems, using methods such as bioprinting and photolithography, and also microfluidics technologies, to allow for realistic co-culture systems and overall tissue organizations (11,12). Overall, such 3D culture systems have the potential to serve as in vitro platforms for cancer studies, with focus on cell-ECM interactions such as ECM remodeling, which consist of changing ECM architecture, degradation and deposition of matrix proteins (2,4,6,13,14).

1.1.1 Importance of Cell-Extracellular Matrix Interactions

An important aspect of tissue function, repair, and diseases such as cancer, is the interplay between the cells and its extracellular matrix (ECM), and evidence demonstrates that the physical and chemical cues from the ECM influence cellular behavior, such as proliferation, differentiation and migration (1,2,5,15).

One of the main receptors connecting cells and the ECM is a group of transmembrane proteins called integrins, which consist of two distinct subunits connected through non-covalent interactions (16,17). They can bind to specific motifs present in the ECM proteins outside the cell, and they bind to the cytoskeleton structures, typically actin, within the cells through intermediate molecules such as talin (2,16,17). These interactions, in turn, relay signals that impact events in the nucleus, such as gene expressions, resulting in modulated protein levels and cell behaviors, indicating the broad mechanism of ECM influence on cellular function and vice versa (1,18–21). Realizing that the ECM provides a complex mixture of cues, including

biochemical and physical, significant efforts have been undertaken to develop systems to assess the effects of individual cues in a high-throughput manner (22–24). In recent examples, one study developed a high throughput approach to modulate matrix stiffness and ligand density separately to obtain different combinations of these parameters, with cell seeding over the hydrogel, and another study employed a high-throughput method for studying cells encapsulated in 3D (23,24).

Among the physical or mechanical cues present during cell-ECM interactions are mechanical stiffness, fiber alignment, and porosity (25–27). The features, cues for mechanotransduction, in turn contribute to the remodeling processes through mechanisms such as protease activities like that of matrix metalloproteinases (MMPs) (2,4,5,28,29). MMPs may be membrane bound or secreted by cells to alter the environment enabling cellular process such as proliferation and migration (5,30,31). Thus, in the case of cancer, ECM undergoes changes from the norm, including through MMP activities, and further triggers the evolvement of tumors towards malignancy (2,32,33).

1.1.2 Importance of Three-Dimensional Microenvironment

Collective evidence has demonstrated the importance of three-dimensional culture systems to better represent physiological conditions (1,6,34). In addition, cancer growth, migration or invasion all occur in a complex 3D microenvironment, and in order to begin to understand cancer behavior and mechanisms of disease progression, especially the role of cell-ECM interaction, culture systems that introduce the third dimension are more likely to yield reliable and clinically-translatable results (6,8,34).

Studies have indicated that normal epithelial cells in 3D, compared to 2D, demonstrate more regular behavior, such as formation of lumen by breast epithelial cells (35). This is an indication that 3D cultures enable having a relative comparison in experiments because there is an expectation for normal and cancerous cells to be more distinctive and behave naturally in 3D cultures in vitro (1,35,36). In one study, behavior of ovarian cancer cells was studied in 2D and 3D (37). Results indicated increased proliferation in a 3D agarose gel compared to cells on a 2D substrate. Additionally, MMP-2 and MMP-9, hypoxia inducible factor-1α (HIF-1α) and vascular endothelial growth factor A (VEGF-A) expressions, quantified by reverse transcription polymerase chain reaction, were greater in 3D relative to 2D (37). Therefore, studies looking at mechanisms or potential therapeutics benefit from having platforms that allow for better physiological mimic as well as retain in vivo characteristics of cell types (8,36).

Additionally, 3D cultures simultaneously allow for co-cultures with spatial control (38,39). This is especially critical for recapitulating cancer environment because of the complex cell-cell interactions occurring between cancer cells and cells within the stroma (3,36). In one such system, spheroids consisting of cancer cells and endothelial cells mixed together were formed and encapsulated within fibroblast-mixed fibrin matrix (40). This system of co-culture demonstrated endothelial cell sprouting to form vessels, and under hypoxic conditions it was shown that cancer cells were more prone to entering the vasculature mimicking intravasation (40). This demonstrates 3D systems enable complex co-culture systems that have been shown to emulate pathophysiological processes, such as the initial steps of metastasis.

1.1.3 Current use of Hydrogels as In Vitro Model Systems

Examples of widely used hydrogels include poly(ethylene glycol), polyacrylamide, alginate, agarose, collagen, fibrin, gelatin methacrylate (GelMA) (41,42). Some degree of control in formation of natural hydrogels have been successfully implemented. For example, the microstructures of collagen hydrogels have been manipulated through temperature-dependent gelation approaches (43). The temperature during the initial gelation phase was shown to determine the fiber diameter and the pore sizes (43). This way, the differences in the ECM structure dictated the invasion of glioma cells in vitro (43). Alternatively, the perceived stiffness of matrigel was altered by changing the height of the hydrogel that was tethered to glass, such that shorter hydrogel heights allowed the cells to perceive increased hydrogel stiffness (44). Despite these benefits of using natural hydrogels, there are issues with consistency and heterogeneity, making it challenging to produce defined culture systems (1,6).

On the other hand, hybrid and completely synthetic hydrogels provide certain degree of consistency in properties, and enable manipulations to the hydrogels to modify those properties (1,42). Progress in chemical modifications and technologies using light-based polymerization also improve the ability to generate controlled cell-ECM interactions and the spatial and mechanical organization of hydrogel structures for various applications, such as hepatocytes and hematopoietic stem cell culture and mechanotransduction studies (45–50). In recent years, the use of gelatin methacrylate (GelMA) has been recognized because its synthesis process is relatively simple, and the overall costs are low, and mainly because it naturally has some cell-binding motifs (51–53). Gelatin is a form of denatured collagen, which represents the one of the most

abundant proteins in the human body (52). Synthesizing gelatin methacrylate, provides additional benefits of crosslinking-based hydrogel formations, including 3D patterning and printing techniques that allow for spatial organization and consequently increased complexity (52–54).

1.1.4 3D Hydrogel Patterning Methods

As previously described, 3D hydrogel constructs have become a critical part of tissue engineering and cancer research, and additionally, the repertoire of technologies that enable complexities within the 3D culture systems have grown over the years. Examples of such technologies include photolithography, micromolding, and bioprinting (12,52). Photolithography can be generally classified into two methods: with or without use of photomasks to determine construct geometries (12). Transparency photomasks containing 2D geometries of interest, function as a selective barrier for UV penetration, and hydrogels that can form through UV polymerization can be used to form constructs with spatial and geometric control (12,54–56). Several studies have demonstrated this approach to create 3D constructs, and in one of the initial studies that applied this approach, the setup involved adding a precursor solution with photoinitiator to a mold, or an enclosed volume, that holds the solution during its polymerization with spatial selectivity, dependent on the photomask design (11,55).

Photolithography methods that do not involve photomasks, instead utilize devices that produce 3D structures based on computer-aided design model input and medical imaging information to recreate 3D tissue structure (12,57). For stereolithography, there are laser-based approaches, where UV laser light is introduced

in specific spatial patterns to crosslink the material (12,57). Both bottom-up and top-down approaches have been implemented, each depending on the method of layer formation (57). Within these approaches, is a concept called digital light projection, using Digital Micro-mirror Decive™, where individually controlled series of mirrors are used to crosslink a single layer at the same time (57). 3D bioprinting of hydrogels with encapsulated cells has been an alternative approach in the field of 3D patterning for tissue engineering applications (12). Similar to photolithography, the hydrogels can be formed through photopolymerization, and additionally, because the patterns are "deposited" continuously, they can also be thermally and chemically crosslinked as they are added (58). This method is also amenable for first constructing a template around which hydrogels can be formed (58).

1.1.5 Cancer and ECM Remodeling

Cancer is characterized by uncontrolled proliferation of cells and their potential to migrate through tissue and metastasize to secondary sites (4,59–62). The initiation of cancer is generally attributed to damaged DNA and genetic changes in cells, and defective apoptosis, leading to uncontrolled proliferation and formation of tumors (60,62–64). In recent years, studies have demonstrated that physical properties, such as matrix stiffness or mechanical resistance, and alignment of extracellular matrix fibers in the tissue, and chemical cues, such as cytokines and other secreted factors from the microenvironment, play a significant role in cancer cell proliferation, migration and metastasis (26,32,33,60,61,65–69).

Cancer cells/cancer associated stromal cells are known to remodel the matrix by degrading the ECM, depositing their own ECM, and thereby changing the properties of their environment (26,44,70). One of the main readouts of remodeling is the ECM mechanical properties, and one of the ways these changes are medically determined is through elastography (71–73). Elastography is based on the concept of force application and deformation detection, which then provides information about the material properties of the tissue (73,74). The deformation detection is generally done through imaging techniques such as ultrasound, and abnormalities in the material properties within a tissue has been used as a diagnostic tool (74).

Therefore, there has been extensive research into studying remodeling of the cancer environment and the cellular responses. In one study, cancerous tissues were studied using atomic force microscopy (AFM), and the stiffness of individual components were assessed in the context of whole tissue, as opposed to considering just isolated cells or ECM (75). In literature, other methods such as second harmonic generation (SHG) microscopy, particle tracking microrheology (PTM) and particle imaging velocimetry (PIV) are also used for detecting changes in extracellular matrix, with SHG primarily used for collagen matrices (14,32,76). SHG microscopy is based on nonlinear optics, empirically detecting key parameters such as polarization and nonlinear susceptibility (77–80). Only certain types of structures can be used to image using SHG, one being collagen I (78). Simply, the process involves interaction of two low energy, high intensity photons, which interact with the material, and form waves with frequency totaling the sum of the initial lower frequencies (80).

Multiple-particle tracking, PTM and PIV approaches have become more diversified and useful in studying cell-ECM interactions, through detection of ECM deformation and changes in its mechanical properties within in vitro systems (13,14,44,76,81,82). In general, for PTM, particles' Brownian motions are monitored over time, and trajectories are used to determine particles' mean square displacement, leading to the determination of the rheological properties of materials (82). Studies have extended particle tracking methods to study time-dependent changes in properties of the ECM and cellular interactions with the ECM (13,14,81). PIV-based approach, based on image correlation of defined fields of intensity distributions, has also been applied to systems to assess stresses and deformations in the context of cell-ECM interactions (44,76,83).

1.1.6 Microfluidic Systems for Cancer Research

More recently, great strides have been achieved in incorporating microfluidics platforms to cancer research, and flow systems have been devised to function as cell culture systems, as well as tools for diagnostics, mechanical and biochemical testing (84–88). In order to investigate the effects of hydrostatic pressure on cancer cells, a system was developed to introduce different pressures into a microfluidics chamber with lung cancer cells, and it was determined that the cells were more migratory under higher pressures, and long durations of high pressure resulted in cell volume change, attributed to changes in aquaporin expression (89). This indicates that the higher interstitial fluid pressure present in a cancer microenvironment has effects on the cell phenotype.

One of the highlights of the microfluidics system is its adaptability to various types of biological analysis, because it can also serve as a cell culture platform while allowing for 3D complexity. As an example, a co-culture system, involving cancer and cells from the microenvironment, was established (84). Here, with the intention to mimic bone-metastasized prostate cancer, prostate cancer cells were mixed with osteoblasts and endothelial cells and added into the microfluidic device for spheroid generation and culture (84).

The merging of ECM and microfluidics technology has furthered capabilities in building up the complex cell culture systems to enable more realistic platforms for cancer studies and drug screening efforts (90,91). In one study, patterning of GelMA was extended into a perfusable system consisting of fibroblasts and endothelial cells co-culture (54). To increase complexity, another novel method introduced photomask-based patterning approach to generate homogeneous or co-culture systems with ECM "microtissues" within microfluidics device that enabled continuous perfusion around these microtissues (90,91). In addition, this system included two layers of polyacrylamide hydrogels that served as non-cell adherent surfaces outside the microtissues and also as force-sensors enabling stress measurements (90,91).

1.2 Thesis Objective

Studying any aspect of cancer progression should ideally involve understanding the role of both the cancer cells themselves, as well as the important cues from the tumor microenvironment (60,65). Therefore, techniques that enable creating three-

dimensional (3D) cell-laden structures, with defined spatial organization and ability to co-culture are crucial for modeling and studying different aspects of cancer progression. Various methods such as 3D printing and photo-patterning approaches currently exist (53,55,92). The aim is to establish a simple and modified, yet versatile approach, to encapsulate cells within degradable, spatially-defined 3D structures, allowing single and co-cultures, within defined geometries and confinements.

Here, we aimed to develop a modified approach to existing 3D photo-patterning methods that utilize a transparency photomask that selectively allows for UV light penetration, and therefore allows the generation of defined hydrogel structures. We first optimized this approach by generating acellular constructs made of gelatin methacrylate patterns, with full embedment within a secondary surrounding hydrogel. We next, encapsulated cells within patterned structures, surrounded by a single hydrogel layer, and results demonstrated significant viability of the cells immediately post-encapsulation. Using this approach, we also tested co-cultures formation by adding second cell types to either the surrounding hydrogel layer or by introducing a second set of patterned structures around the initial set. This allows for controlled spatial confinement of the different cell types of interest.

Next, we extended photopatterning into microfluidics devices. The aim was to encapsulate cancer spheroids within a three-dimensional degradable hydrogel, and observe their proliferation and quantify the changes occurring in the matrix. The approach utilized here simply involved pressure application, deformation detection, and assessing time-dependent changes in volumetric strains as a potential measure of changing mechanical properties of the hydrogel structures.

CHAPTER 2: 3D PHOTOPATTERNING OF HYDROGELS WITH DIVERSE AND COMPLEX ARCHITECTURES FOR TISSUE ENGINEERING AND DISEASE MODELS

2.1 Abstract

Techniques that can create three-dimensional (3D) structures to provide architectural support for cells have a significant impact in generating complex and hierarchically organized tissues/organs. In recent times, a number of technologies, including photo-patterning, have been developed to create such intricate 3D structures. Herein, we describe an easy-to-implement photo-patterning approach, involving a conventional fluorescent microscope and a simple photomask, to encapsulate cells within spatially-defined 3D structures. We have demonstrated the ease and the versatility of this approach by creating simple to complex as well as multi-layered structures. We have extended this photo-patterning approach to incorporate and spatially organize multiple cell types, thereby establishing co-culture systems. Such cost-effective and easy-to-use approaches can greatly advance tissue engineering strategies.

2.2 Introduction

The ability to encapsulate cells within biomaterials, like hydrogels, has been widely used to achieve three-dimensional (3D) culture of cells. Significant progress has been made over the years to engineer hydrogel matrices with tissue-specific mechanical and biochemical properties (93–99). Recent times have witnessed a surge of interest in

recapitulating the heterogeneity and architectural complexity of native tissues in hydrogel scaffolds. To this end, a number of patterning and printing techniques have been developed (11,53,92,100–106). Some of these include nozzle-based printing, DMD projection patterning, and laser-based stereolithography to create 3D structures, and methods to introduce required features into preexisting 3D structures (53,100,104,107,108).

Among the 3D patterning methods, the use of stereolithography-based approaches has garnered the most attention due to its versatility and ease of construction. In general, this method spatially restricts the exposure of light into a hydrogel precursor solution enriched with photoinitiators, thereby selectively polymerizing and creating patterned structures that can be controlled spatially. Methods such as DMD projection printing use computer controlled micro-mirrors to selectively reflect light from a UV source to achieve spatially variant gelation of hydrogels (104,109). However, the simultaneous encapsulation of cells within DMD generated scaffolds is a difficult task. Laser-based methods have also been used, especially in applications where cells were incorporated into the scaffold *in situ* during the patterning process. In these approaches, a laser light source is directed and focused towards a precursor solution containing a mixture of cells, polymers containing acrylate groups, and photoinitiator placed on a motorized platform to initiate the gelation process. The programmed movement of the platform generates patterned architectures in the resulting hydrogel (108). In addition to these methods that require specialized technologies and equipment, studies have also employed easily accessible approaches such as preexisting 3D structures and

photomask-based systems to achieve similar results (39,46,55,100,102,103,105,110–115).

In the case of photomask-based systems, a mask with desired patterns is printed onto a transparency such that light only penetrates regions that are not printed on with ink. A variety of approaches have been described using this method, including one where precursor polymer solution mixed with cells was infused into a mold, and polymerized with the mask acting as a selective barrier for UV light. This setup enabled multiple rounds of washing off non-gelled regions, solution infusion, and subsequent polymerization to create 3D patterns. The changes in the photomasks at each step meant different pattern designs can be added, where each new pattern incorporated both the depth of the previous and most recently polymerized pattern(s) (55,103,111). This approach was used to create co-culture systems where one cell type is encapsulated within patterned structures while the second cell type is confined within the surrounding hydrogel (39). These mask-based methods were further diversified through efforts using hydrogel polymerization that is inversely dependent on UV intensity exposures based on degree of transparency on photomask. Thus patterned porosity within the hydrogel could be generated (112). Using the overall photomask approach, a visible light-based photopolymerization of multiple layers with different designs using lasers was also achieved with added benefits of chemical tethering of different layers (113).

The merging of 3D patterning with stem cells and biomaterials has undeniably provided researchers new prodigious tools to create complex tissues. The wide spread application of such approaches, however, relies on easily adaptable and easy-to-devise protocols. To this end, we have integrated a photomask-based stereolithography

approach coupled with the photopolymerization of precursors to create patterned 3D structures reinforced with a surrounding hydrogel layer. As a proof-of-concept, we have created a wide variety of mechanically robust micro- and macro-scale structures with simple to complex architectures. We have also demonstrated their use in cell culture.

2.3 Materials and Methods

2.3.1 Synthesis and Purification of Gelatin Methacrylate (GelMA)

Gelatin methacrylate (GelMA) was synthesized as described previously (116). In short, 10 g of bovine skin, Type B, gelatin (Sigma Aldrich) was added to 100 ml phosphate buffered saline (PBS; Gibco) to obtain a 10%(wt/v) solution and stirred at 60˚C for a minimum of 30 minutes to achieve complete dissolution. Around, 8 ml of methacrylic anhydride (MA, Sigma Aldrich) was added dropwise to the gelatin solution at a rate of 0.5 ml/min. This continuously stirred solution was brought to 50˚C, reacted for 1 hour, and quenched by addition of a 2x dilution of warm PBS. This was dialyzed against Milli-Q water using dialysis tubing with a 12-14 kDa cutoff (Spectrum Laboratories) for one week (3 times/day water change) at 40˚C to remove the excess reactants. The GelMA solution was filtered, frozen down, and lyophilized for four days. Prior to cellular encapsulation, the dried GelMA was further purified using a Sephadex G-25 column (GE Healthcare Life Sciences) and re-lyophilized.

2.3.2 Synthesis and Purification of Poly(ethylene glycol)-diacrylate (PEGDA)

Poly(ethylene glycol)-diacrylate (PEGDA) was prepared as previously described (117). Briefly, 5.29 mmol of poly (ethylene glycol) (18 g of 3.4 kDa; Sigma Aldrich) was dissolved in 300 mL of toluene at 127°C and kept under reflux for 4 hours with vigorous stirring. To remove trace amounts of water, the solution was subjected to azeotropic distillation. 180 mL of anhydrous dichloromethane was added at room temperature, and subsequently, 1.623 mL (11.64 mmol, 2.2 equivalents) of triethylamine was added under vigorous stirring. The reaction mixture was transferred to an ice bath to further cool it down. Upon cooling, 0.942 mL (11.64 mmol, 2.2 equivalents) of acryloyl chloride mixed in 15 mL of anhydrous dichloromethane was introduced dropwise to the mixture at 4˚C over 30 minutes. The reaction was kept for 30 more minutes at 4˚C before increasing to 45˚C overnight. The reaction mixture was filtered through diatomaceous earth to remove quaternary ammonium salts. The filtrate was concentrated using a rotary evaporator and precipitated in excess diethyl ether. The precipitated product was redissolved in dichloromethane and reprecipitated in diethyl ether. The resultant PEGDA was filtered and dried under vacuum at room temperature for 24 hours. The dried PEGDA was further purified using a Sephadex G-25 column (GE Healthcare Life Sciences) and lyophilized.

2.3.3 Synthesis of Lithium phenyl-2,4,6-trimethylbenoylphosphinate (LAP)

Lithium phenyl-2,4,6-trimethylbenoylphosphinate (LAP) was prepared as previously described (118). 2,4,6-trimethylbenzoyl chloride (Alfa Aesar) was

introduced dropwise to an equal molar of dimethyl phenylphosphonite (Alfa Aesar) while stirring at room temperature under argon. After 18 hours, the temperature of the reaction mixture was increased to 50˚C. Lithium bromide, mixed in 2-butanone, was added in excess, resulting in precipitation within 10 minutes. Upon precipitation, the temperature was once again cooled to room temperature for another 4 hours. The precipitate was collected via filtration, and washed thrice using 2-butanone to ensure complete removal of excess lithium bromide. The product was dried under vacuum to remove excess 2-butanone, to yield LAP.

2.3.4 Methacrylation of glass coverslips

The glass surface was methacrylated according to the manufacturer's protocol. Briefly, 15 mm diameter glass coverslips were treated with 2.5 M NaOH solution for 30 minutes before rinsing in DI water, and dried under airflow. A dilute solution of glacial acetic acid was prepared in DI water at a ratio of 1:10. A working solution containing 200 µL of ethanol, 1 µL of 3-(trimethoxysilyl) propylmethacryalte (Sigma Aldrich), and 6 µL of the diluted acetic acid was prepared. The cleaned glass surfaces were treated with this working solution for 6 to 10 minutes prior to rinsing with pure ethanol for 10 minutes. The coverslips were dried under airflow and incubated in 60°C for 2 hours. The coverslips were used within 24 hours.

2.3.5 PLL-PEG coated Coverslips

12 mm or 15 mm diameter coverslips, or 22 x 22 mm square coverslips were treated with 100% ethanol for 15 minutes and dried under gentle airflow. The cleaned

glass surfaces were exposed to UV/Ozone for 6 minutes and were immediately treated with 0.1 mg/mL PLL-PEG (Surface Solutions), diluted in PBS from a stock solution with a concentration of 5 mg/mL. After 30 minutes of PLL-PEG treatment, the coverslips were rinsed in distilled water and were dried through aspiration. PLL-PEG coated coverslips were used within 24 hours.

2.3.6 3D Patterning of Structures

The designs of interest were generated using the software AutoCAD. The file was then sent to CAD/Art Services, Inc, who generated the corresponding transparency photomask. The photomask along with a collimated light was used to selectively polymerize the desired structures. Specifically, the photomask was placed directly on the stage of an inverted microscope. A photopolymerizable solution (here GelMA with LAP), which was sandwiched between two coverslips was placed directly on the photomask and polymerized with collimated UV light (Supplementary Fig. S2.1).

2.3.7 Embedded 3D Patterning

A known weight of GelMA powder was added into a known volume of PBS to create 10% wt/v solution. The GelMA in PBS solution was vortexed at room temperature to dissolve the polymer. The resultant mixture was transferred to a 60 °C water bath for 15 minutes and vortexed for an additional minute at room temperature. This process was repeated once more to achieve complete dissolution of the GelMA in PBS. Once completely dissolved, the solution was brought to 37 °C and used to create acellular and cell-laden hydrogel structures.

The 10% wt/v GelMA solution was supplemented with the photoinitator LAP and 200 nm diameter green fluorescent particles at concentrations of 2mM and 1% v/v, respectively. A 22 x 22 mm square coverslip was cleaned in DI water and dried prior to adding the precursor solution onto the surface. A PLL-PEG treated 12 mm coverslip was gently placed on top to sandwich the solution between the two glass surfaces.

A transparency photomask containing dark background and clear patterns was placed onto the microscope stage and positioned under bright field such that the desired pattern is centered over the eyepiece. The GelMA solution between the coverslips was placed onto the mask and photopolymerized using a collimated UV light source, which was generated by passing the light from an X-Cite Mercury lamp through a conventional DAPI channel filter cube with excitation and emission centered around 358 nm and 463 nm, respectively. The gelled construct was transferred to a petri dish filled with 37°C PBS and the solution was pipetted gently yet repeatedly between the glass coverslips to remove the unpolymerized GelMA solution and detach the PLL-PEG treated coverslip. The resulting GelMA structures were temporarily stored within a PBS solution.

PEGDA (Mn: 3400) was dissolved in PBS to achieve 10% wt/v along with 2 mM LAP and 1% wt/v of 200 nm diameter red fluorescent particles. The GelMA structures attached to the square coverslips were retrieved and the excess liquid was aspirated prior to the addition of the PEGDA precursor solution onto the GelMA patterns. A 15 mm diameter methacrylated coverslip was gently placed on top and was polymerized as previously described. The coverslip was transferred into a PBS solution afterwards and the gelled construct tethered onto a methacrylated coverslip was

retrieved. The hydrogel composite structure, with GelMA and PEGDA, was stored within a PBS solution.

To complete the enclosure of the GelMA features within the PEGDA hydrogel, PEGDA precursor solution was aliquoted onto a 22 x 22 mm square coverslip. The patterned construct was retrieved and the excess liquid was removed prior to placing the hydrogel surface onto the precursor solution. After photopolymerization and removal of the cover slip, the supported 3D constructs tethered onto 15 mm diameter coverslips were obtained.

2.3.8 Free-standing photo-patterned scaffolds

The GelMA patterns were constructed on 22 x 22 mm square coverslips and were incubated in PBS as described in *Embedded 3D Patterning*. PEGDA was dissolved in PBS to obtain a solution containing 10, 20, or 30% wt/v along with LAP (concentration of 2 mM). The coverslips containing the patterns were removed from PBS and the excess liquid was aspirated. The PEGDA solution was added onto the patterns and a 15 mm diameter PLL-PEG coated coverslip was placed on top. The precursor solution was photopolymerized and the resulting gel was incubated in PBS for 5 minutes at room temperature. The PLL-PEG coated coverslip was mechanically removed. The GelMA construct remaining on the square coverslip was carefully detached to yield a free-standing scaffold.

2.3.9 Multi-layered scaffolds

The methodology resembles the procedure discussed in *Embedded 3D Patterning* however with significant modifications. To create the first layer of the scaffold, 22 x 22 mm square coverslips were coated with PLL-PEG while the 15 mm diameter circular coverslips were methacrylated. This resulted in GelMA structures covalently bonded to the circular coverslip. GelMA precursor solution supplemented with 2 mM LAP was added onto the PLL-PEG coated square coverslip prior to placing the circular coverslip onto the solution submerging the GelMA structures. The construct was photopolymerized and the circular coverslip was removed. The above process was repeated to construct supporting layers and additional patterned layers.

2.3.10 Cell Culture and Encapsulation

Human mesenchymal stem cells (hMSCs), human fibroblasts, and MDA-MB 231s (breast cancer cell line) were cultured in growth medium comprised of 1% Penicillin/streptomycin, 1% L-Glutamine, 10% Fetal Bovine Serum (Gibco), and 88% DMEM (HyClone®, Thermo Scientific). Human umbilical vein endothelial cells (HUVECs) were cultured in medium (HUVEC medium) composed of 1% Sodium Pyruvate (Life Technologies), 1% Penicillin/Streptomycin, 10% Fetal Bovine Serum (Gibco), 10% Endothelial Cell Growth Medium (Gibco) and 78% M199 (Gibco).

To label the cells, they were trypsinized and resuspended in 7 μM green or red CellTracker dyes (Molecular Probes®, Life Technologies) or 1 μg/mL of Hoescht 33342 (Life Technologies) dissolved in OPTIMEM (Gibco). After 20 minutes of incubation, the cells were washed multiple times with PBS.

During the cell encapsulation, a cell pellet, containing between 2-6 million cells, was resuspended in 100 µL of 10% GelMA precursor solution supplemented with 2 mM LAP and 0.01% ascorbic acid. The cells were patterned following the procedure discussed in *Free-standing photo-patterned scaffolds* until the step where cell-laden GelMA patterns were embedded with an additional hydrogel layer. Here, the construct was not detached from the glass. Though we use both GelMA and PEGDA to create the surrounding hydrogel layer, in the ones shown in Fig. 4 the hydrogel layer used was GelMA. The cell-laden constructs were incubated in sterile PBS containing 2% Pen/Strep for 5 minutes at 37 °C prior to replacing the solution with growth medium. The co-cultures involving HUVEC cells were cultured in HUVEC medium.

2.3.11 Live/Dead Assay of Cellular Constructs

The cell-encapsulated constructs were first washed three times with PBS, and subsequently incubated in a Live/Dead solution (500 µl DMEM containing 0.25 µL of Calcein AM, 1 µL of Ethidium homodimer-1, Life Technologies) for about 30 minutes at 37 °C. After incubation, the constructs were once again washed thoroughly with PBS to remove residual dye, and imaged using fluorescence microscopy.

2.4 Results

2.4.1 Scaffold fabrication

GelMA solution of 10% wt/v was used for the fabrication of 3D-patterned hydrogel structures of varying shape, size, height, and complexity. The formation and

optimization of the structures were carried out using fluorescent particles of 200 nm diameters suspended in GelMA solution allowing easy visualization of the resulting structures. Furthermore, we tested the cytocompatibility of the described fabrication procedure for various cell types (hMSC, HUVECs, human fibroblasts, MDA-MB 231). Both homogeneous and co-culture systems were implemented.

2.4.2 Embedded 3D Patterning

The GelMA solutions supplemented with LAP and fluorescent particles were sandwiched between PLL-PEG treated and regular coverslips (Fig. 2.1A), which was exposed to a collimated UV light through a photomask printed with the desired patterns. The PLL-PEG treatment was used to promote adhesion of the hydrogel onto the regular coverslip. The non-irradiated regions were then washed off to leave behind the 3D patterned GelMA structures (Fig. 2.1B). To embed the 3D patterned structures within a hydrogel, the GelMA structures formed onto the glass coverslip was immersed within PEGDA precursor solution and photopolymerized, where the PEGDA solution was sandwiched between the GelMA layer and a methacrylated glass coverslip prior to gelation (Fig. 2.1C). The use of methacrylated coverslip ensures the detachment of the GelMA structures after they are embedded within the PEGDA hydrogels. To achieve the complete embedment of the GelMA structures, the above-mentioned procedure was repeated using a glass coverslip that was not methacrylated (Fig. 1D). Though the results describe the use of PEGDA to create the surrounding layer, any photopolymerizable biomaterial could be used. We have validated the use of PEGDA and GelMA towards this patterning approach.

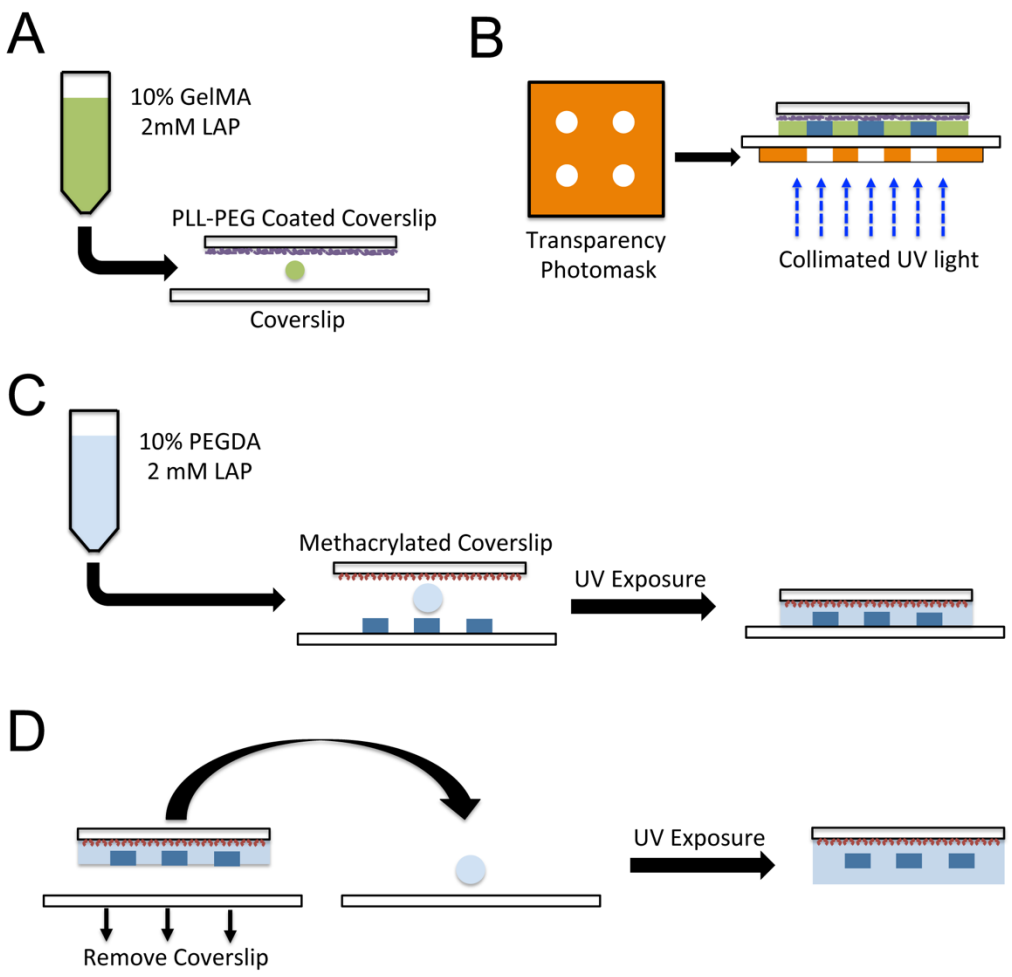

Figure 2.1: Schematic representation of the protocol for generating three-dimensional patterned structures. (A) The GelMA solution was sandwiched between a PLL-PEG coated coverslip and a non-treated coverslip. (B) The sandwich was exposed to collimated UV light with a transparency photomask to selectively block the light reaching the GelMA solution. (C) Precursor solution, consisting of PEGDA, was added onto the patterned structures and sandwiched with a methacrylated coverslip prior to exposing to UV. (D) To completely embed the patterned GelMA structures, PEGDA solution was sandwiched between a coverslip and the previous structure from (C) and exposed to UV.

2.4.3 Varying the height and size of the 3D patterned structures

The photo-patterning process described here can be used easily to vary the height and sizes of the patterned structures. The height of the structures can be easily adjusted by varying the volume of GelMA precursor solution sandwiched between the cover slips. By photopolymerizing volumes of 8, 14, and 20 μL of GelMA solutions, we fabricated cylindrical structures with heights of approximately 47, 103, and 115 μm, respectively (Fig. 2.2A). Figure 2.2A depicts the z-stack confocal images of the cylindrical hydrogel structures of different heights. The X-Y cross-sections show the circular GelMA structures, embedded with green fluorescent beads, surrounded by PEGDA hydrogels embedded with red fluorescent beads (Fig. 2.2A Top Panel). The confocal images in X-Z plane show the increase in height of the GelMA structures encased within the PEGDA layer with increase in the volume of the GelMA precursor solution (Fig 2.2A Bottom Panels). The images of GelMA with green beads and PEGDA with red beads have been merged to demonstrate the embedment of GelMA structures within a PEGDA hydrogel. The size of the structures can be controlled by altering the size of the patterns on the photomasks. Figure 2.2B illustrates X-Y cross-sections of the circular structures with increasing diameters of approximately 80, 160, and 250 μm. In addition to circles, we have also created other basic geometries such as triangles and squares. The 3D reconstructed images from the z-stack volumes of these structures are depicted in Fig. 2.2C. Since the 3D structures are mechanically supported by the PEGDA hydrogels, we can generate free-standing scaffolds containing embedded 3D patterned GelMA structures. The mechanical properties of the PEGDA hydrogels increase with increasing precursor concentration (119). By tuning the concentration of

the PEGDA hydrogels from 10% to 30%, we can vary the mechanical properties of the hydrogel surrounding the GelMA structures (Fig. 2.2D).

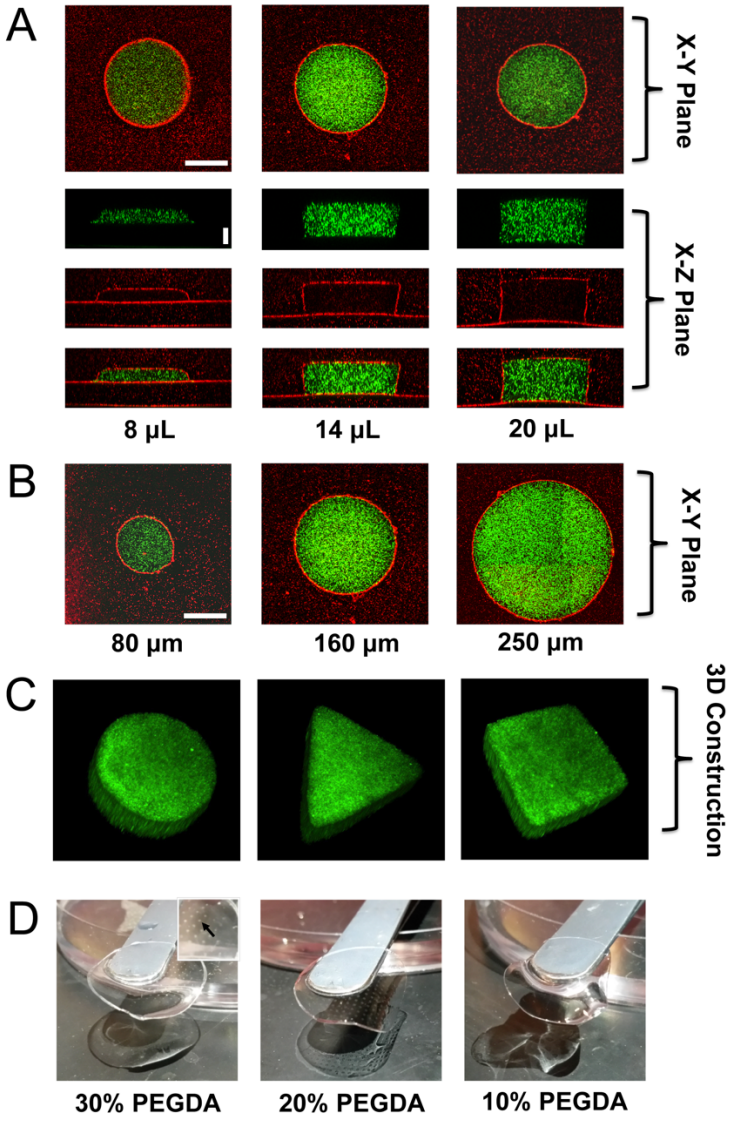

Figure 2.2: Optimization and characterization of patterned structures. (A) The height of the patterned features was adjusted by changing the volume of the GelMA solution from 8 to 20 µl prior to gelation. Horizontal scale bar: 100 µm. Vertical scale bar: 50 µm. (B) Cylindrical patterns with increasing diameters of 80, 160, and 250 µm were generated by altering the design on the photomask. Scale bar: 75 µm. (C) 3D reconstruction of the GelMA structures with different extruded shapes — circular, triangle, and square. (D) Free-standing patterned GelMA structures surrounded with a PEGDA hydrogel with varying PEGDA concentration (30-10%). The inset shows the GelMA patterns within the PEGDA hydrogel, with the arrow provided for easy identification.

2.4.4 Generating complex and multi-layered structures

We have extended the photo-patterning process to create large, complex structures. To this end, we employed image processing techniques on available images of Isaac Newton to generate a binary image suitable for the photomask. Employing this photomask and following the protocol described in materials and methods, we have created a 3D patterned portrait of Isaac Newton in GelMA structures embedded within the PEGDA hydrogels (Fig. 2.3A). We employed a similar approach to recreate, in hydrogel form, the vascular network observed in the kidney based on a figure from Marxen, et al (120). Figure 2.3B shows the X-Y cross-section depicting the vascular network structure made of GelMA with the surrounding PEGDA structures.

We have also created multi-layered, supported structures using this approach. Specifically, we generated a bilayer scaffold consisting of line patterns of approximately 100 μm width, with spacing of 500 μm (Fig. 2.3C). X-Y confocal sections of the structure at various Z planes indicate two different GelMA line patterns perpendicular to each other. The X-Z cross-section of this multi-layered structure indicates that the two GelMA lines are integrated at the interface between the layers. One of the current caveats of multi-layered patterning approaches is the lack of structural stability with the additional stacks often leading to structural collapse. In our study, we did not observe any such collapsing of the GelMA upper layer irrespective of the distance between the line GelMA structures in the lower layer. This is mainly due to the supporting hydrogel, which provided the mechanical integrity and support to the patterned GelMA structures and thereby circumventing the inherent mechanical instability. Figure 2.3D shows the 3D reconstructed images of the bilayer patterns.

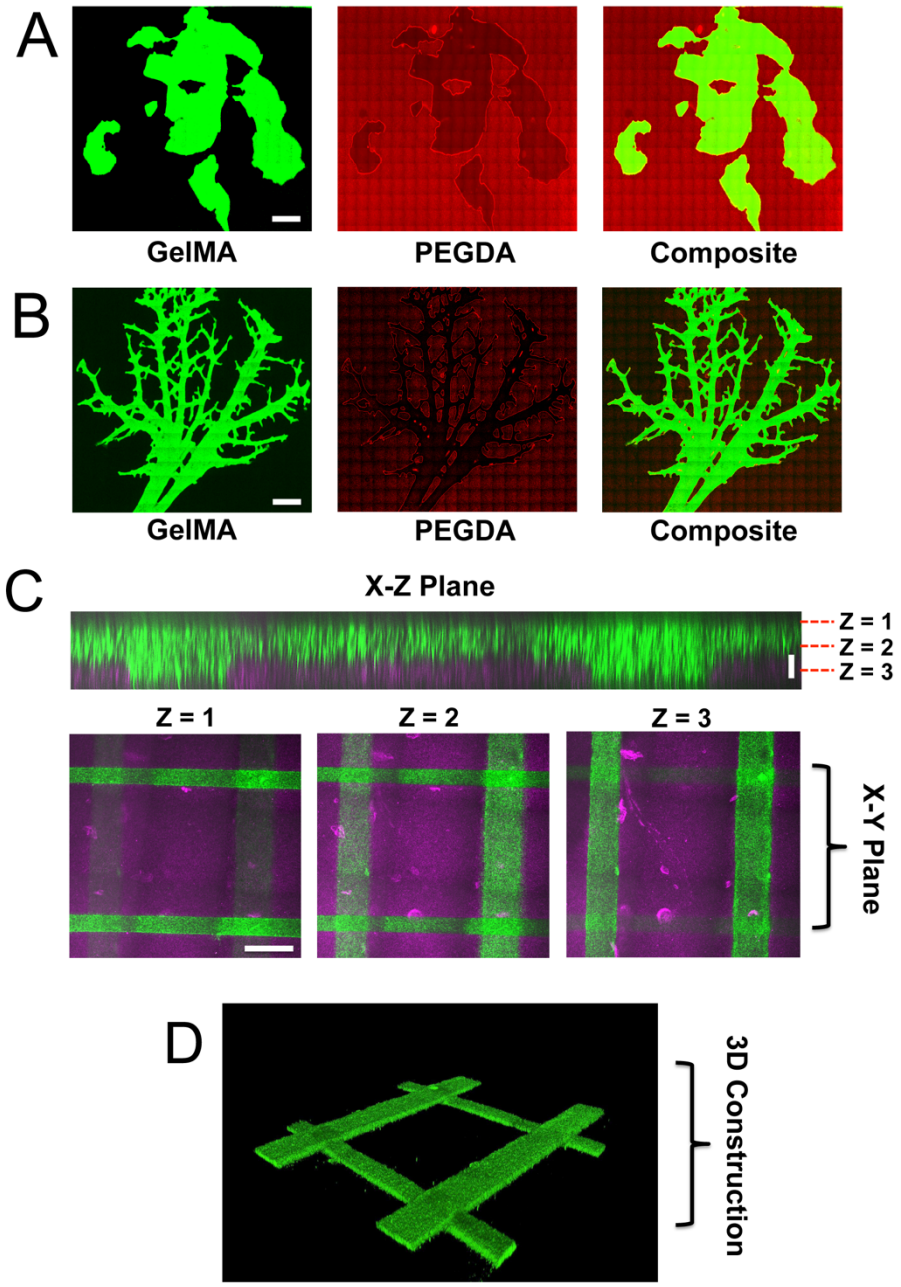

Figure 2.3: Generation of complex patterns. GelMA patterns of (A) Sir Isaac Newton and (B) kidney vasculature. Scale bar: 500 μm (C) Confocal sections of bi-layer hydrogels containing line patterns showing the X-Z plane and X-Y planes at indicated z positions. Horizontal scale bar: 150 μm. Vertical scale bar: 25 μm. (D) 3D reconstruction of the GelMA structures in the bilayer constructs.

2.4.5 Cell Encapsulation

We encapsulated multiple cells within the GelMA structures to assess the cytocompatibility of the 3D photo-patterning technique. Figure 2.4A demonstrates the viability of hMSCs encapsulated within a cylindrical patterned structure of approximately 250 μm diameter surrounded by another hydrogel layer. The cells were labeled with green dye prior to encapsulation to visualize their distribution within the patterned structure (Fig. 2.4A left column). Live-dead analyses of the encapsulated cells indicate that majority of the cells remain viable post-encapsulation (Fig. 2.4A right column). A similar encapsulation experiment was also performed with the bilayer line structures. The hMSCs were encapsulated in both the top and bottom line structures (Fig. 2.4B). Similar to the cylindrical patterns, majority of the cells within the line patterns were found to be viable (Fig. 2.4B right column).

We next determined the ability of the cell-encapsulation within 3D patterning to create spatially distinct co-culture systems. To this end, we have encapsulated HUVECs and MDA-MB-231s where MDA-MB-231 cells were first encapsulated within cylindrical patterns, and HUVECs were encapsulated within the hydrogel layer surrounding the initial patterns. The images obtained from live/dead assay performed three days post-encapsulation illustrates the dense cluster of cancer cells within the circular regions with sparse distribution of surrounding HUVECs (Fig. 2.4C). Secondly, another approach to co-culture, relying on alignment of the photomask, was performed with HUVECs and human fibroblasts, where the two cell types were encapsulated in a spatially confined manner, both within cylindrical 3D patterned structures. The cells were labeled with fluorescent dyes prior to their encapsulation. The HUVECs, shown

in red, and fibroblasts, shown in green, were spatially confined in distinct and alternate positions by photopolymerizing GelMA solutions containing the respective cells in a two-step process (Fig. 2.4D).

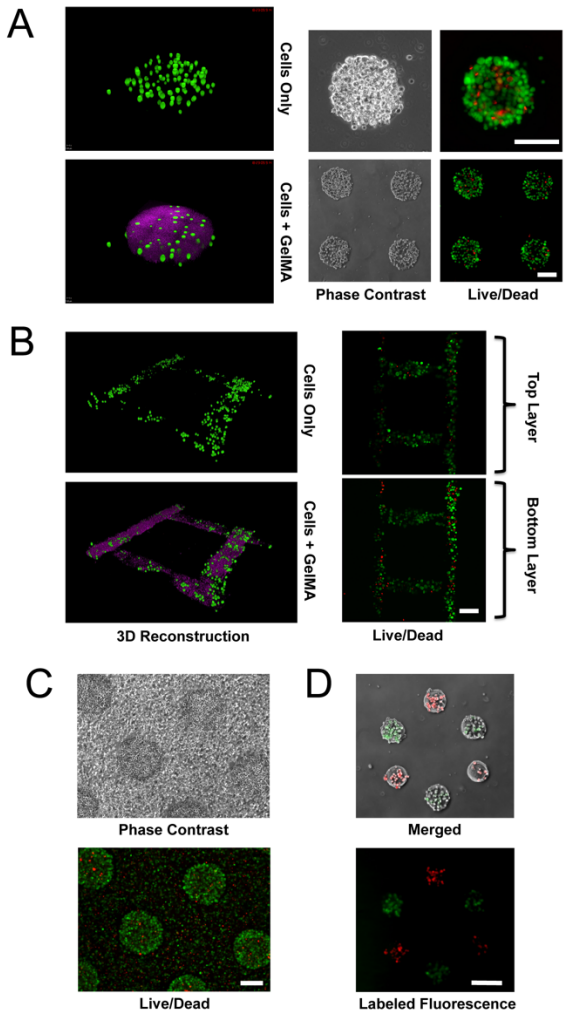

Figure 2.4: Encapsulation of cells. (A-B) 3D reconstruction of cells within the patterned hydrogel and the surrounding GelMA hydrogel layer (Left Column), where the cells were fluorescently labeled with green cell tracker. (Right column) Phase contrast and Live/Dead image of the cylindrical patterns, and Live/Dead images of distinct layers of the bi-layer structures. In live/dead images the green cells indicate viable cells while the red indicates non-viable cells. Scale bar for (A): 200 μm. Scale bar for (B): 150 μm. (C) Co-cultures of HUVEC and MDA-MB-231 cells, where the MDA-MB-231 cell-laden GelMA cylindrical structures are surrounded by hydrogels containing HUVECs. Phase contrast image (top) along with corresponding live/dead image (bottom). Scale bar: 200 μm. (D) Phase contrast and the fluorescently-labeled fibroblasts and HUVECs (bottom) spatially patterned within cylindrical GelMA structures. For easy visualization, the cells were labeled with dyes, with HUVECs represented as red and fibroblasts represented as green. Scale bar: 200 μm.

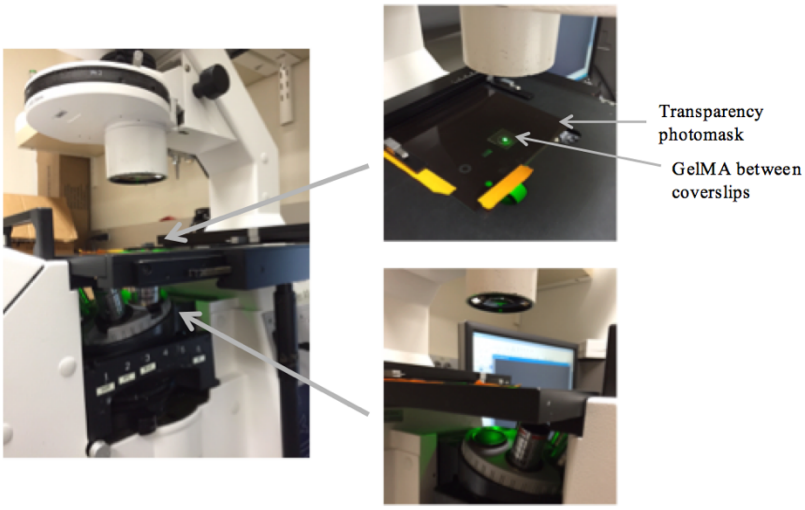

Supplementary Figure S2.1. Experimental Set up for Photopatterning. The GelMA solution, sandwiched between two coverslips, is selectively polymerized using a specific pattern on the transparency photomask using UV light. The effect of using a photomask in between the light source and GelMA is represented by the green light that penetrates through only the desired patterned region on photomask.

2.5 Discussion

Advances in bioprinting have led to the advent of a broad range of approaches to create hierarchical 3D structures with and without cells. However, the widespread use of this technology has been limited due to the requirement of sophisticated equipment and expertise. Herein, we demonstrated an easy to adapt biofabrication technique, which can be used to create 3D structures with varying height, size, shape, and complexity.

When encapsulated, the cells were found to be viable within these structures. Both GelMA and PEGDA are biocompatible and have been extensively used for 3D cell culture systems (39,95,99,116,118). In this study, we opted to encase the patterned structures within a continuous, or non-patterned, surrounding hydrogel layer. Besides providing mechanical integrity and ease of handling, the surrounding hydrogel layer could be doped with biochemical cues and other cells types to create morphogenic gradients and heterotypic cell-cell interactions. Particularly if one chose to engineer integrated tissues within the patterned structures and encapsulate the HUVEC cells within the surrounding hydrogel layer that could lead to vascularization of the tissues.

Figures 2.4C and 2.4D were constructed as a proof of concept co-culture systems because a number of studies have shown the importance of homo- and hetero-typic cell-cell interactions (121,122). Though the demonstration involves only two cell types, the process can be used to encapsulate many more cell types within the same system without overexposing majority of the cells to UV. In addition to the cell phenotype and cell density, the distance between the 3D structures confined with the cells can be easily

varied to create morphogen gradients to study the impact of cell-cell communication through soluble factors.

While the photo-patterning process described in this study offers an easy-to-use and highly adaptable method to create 3D structures with various architectures, the method suffers from a few limitations compared to 3D printing. The technique's dependence on the photomask to extrude patterns with multiple features of varying size could affect the resolution of the structure dimensions, especially for structures with multiple intricate features such as in Isaac Newton's portrait. Since small features require more polymerization time, when larger features are extruded together with these small features, they tend to "over-polymerize" as radicals diffuse outwards from the polymerization site at UV exposure durations required for the smaller features to form. On the other hand, shorter durations required to polymerize large features may be insufficient for the smaller features to form. Thus, when a single gelation time is used for the entire pattern, it is possible for the features' results in GelMA patterns to not coincide with the dimensions of design on the photomasks. In addition, there are limitations to the overall height of the patterns since the coverslip placed onto the large volume of the precursor solutions could tilt resulting in features with uneven heights. Nonetheless, the photo-patterning methodology described in this study offers sufficient promise for homogenous and multi- cell cultures requiring spatial organization in 3D. Since the protocol relies only on a photomask and collimated UV, it could be easily adapted. Such technological platforms could be used to study cell-matrix and cell-cell interactions in a defined 3D environment and to create hierarchical cell-laden structures to engineer complex tissues.

2.6 Acknowledgements

Chapter 2, in full, is a reformatted reprint of the material as it appears in Tissue Engineering Part C Methods, Nov; 21(11):1188-96, 2015. "Embedded 3D photo-patterning of hydrogels with diverse and complex architectures for tissue engineering and disease models." Davey, Shruti Krishna*; Aung, Aereas*; Agrawal, Gaurav; Lim, Han Liang; Kar, Mrityunjoy; and Varghese, Shyni. The thesis author was a primary investigator and author of this paper.

The authors acknowledge Jomkuan Theprungsirikul for her assistance with taking the photographs. Research reported in this publication was supported by the National Institute of Arthritis and Musculoskeletal and Skin Diseases of the National Institutes of Health under Award Number R01 AR063184-02 and the California Institute of Regenerative Medicine (grant RT3-07907). Aereas Aung would like to acknowledge the support from Ruth L. Kirschstein National Research Service Award NIH/NHLBI T32 HL 105373, and ARCS Foundation. The authors also acknowledge the University of California San Diego Neuroscience Microscopy Shared Facility funded through NS047101. The hMSCs used in this study were provided by the Institute for Regenerative Medicine, Texas A&M University, through Grant P40RR017447 from the National Center for Research Resources (NCRR) of the NIH.

CHAPTER 3: NOVEL APPROACH TO QUANTIFY THE DYNAMIC MATRIX MECHANICAL PROPERTIES DURING CANCER GROWTH

3.1 Abstract

The mechanical properties of a cancer microenvironment are known to play a critical role in cancer progression, and therefore, having methods to understand the changes in these properties are of great value. We have developed a novel approach combining 3D photopatterning technique with microfluidics technology to encapsulate a cancer spheroid within a Gelatin Methacrylate (GelMA) hydrogel embedded with fluorescent particles, monitor the cancer growth, and quantify the corresponding changes in the rigidity of the surrounding extracellular matrix (ECM). Here, we applied hydrostatic pressure to compress the cell-laden GelMA hydrogel and recorded the changes in the local volumetric strain throughout culture time. By comparing these empirical results to a finite element simulation, we aim to deduced the approximate changes in the material properties during the cancer growth

3.2 Introduction

3D matrices have proven essential for understanding the importance of matrix mechanical properties in cancer growth. For example, the extent of spheroid growth, and cellular packing density, within agarose gel was shown to be affected by the solid stress in the external matrix (123). Similarly, the mechanical stress distribution has been shown to affect the growth patterns of the cells within these agarose gels, such that the growth is more prevalent in the direction of lower mechanical resistance (67). In another

study that encapsulated cancer cells within deformable alginate capsules of defined radii and shell thicknesses, it was shown that the capsules with thick walls provided confinement to growth, greatly slowing down proliferation after reaching confluence (68). These confinements, relative to free suspension, yielded organization of spheroids with necrotic core, and highly migratory phenotype of the cells at the edges of the spheroids (68). A recent study also demonstrated time-dependent cell growth differences in increasing stiffnesses of alginate gels (124). Here, initially, intermediate stiffness gels produced larger spheroids, but after 13 days, the spheroids in the stiffest gel yielded larger volumes (124). These studies, taken together, portray the significance of a spatial confinement, and how it affects cell behavior, specifically the limitations on growth and in promoting migratory behavior. Additionally, they demonstrate the value in developing in vitro systems that allow for versatile and systematic testing of cell behaviors.

To fully appreciate the role of mechanical resistance, the degradability of native tissue around proliferating cancer cells, where they are capable of degrading the environment using matrix metallo-proteinases (MMPs) has to be considered. Secreted MMPs and membrane bound MMPs play important roles in cancer proliferation and invasion, and in vitro systems have shown its effect on the extent of proliferation (44,125–127). A study that considered the role of mechanical resistance on cell proliferation in a degradable matrix, observed lower proliferation at higher stiffness (126). Further, MMP activity was demonstrated to affect growth, when spheroid size and proliferation comparisons showed smaller spheroids with inhibited MMP activity relative to control samples with no such protease activity inhibition (126).

Studies have also assessed certain changes in the microenvironment properties using particle-tracking methods, such as particle tracking microrheology (PTM) (14,81). The measurements of rheological properties as well as stresses around cancer growth and invasion demonstrated time dependent changes in the surrounding microenvironment and traction forces around invasive cells (14,81). These studies indicate that the cells affect their microenvironment both through applied stresses and by changing the microenvironment properties. This growing appreciation for the complexities involved in cell-matrix interactions underscores the need for studying the responses of cancer cells to their surrounding mechanical cues.

3.3 Materials and Methods

3.3.1 Cell culture

MCF7s (breast cancer cell line) were cultured in growth media and passaged approximately every 3 days. The growth media consisted of 10% fetal bovine serum (FBS, Gibco), 1% penicillin/streptomycin, 1% L-glutamine, and 88% DMEM (HyClone®, Thermo Scientific).

3.3.2 Cancer spheroid formation

MCF-7 cells were trypsinized and counted. Approximately 0.75 million cells were suspended in 4mL growth media. This suspension was added to a non-adherent petri dish, and placed on a shaker with 45rpm. Spheroids were cultured this way for at least 2 to 3 days, and were used subsequently for encapsulation.

3.3.3 Microfluidics Device Preparation

The microfluidics chip device was prepared as previously described (90,91). First, a 24x50 mm glass coverslip and a 12 mm diameter circular coverslip were methacrylated with a solution consisting of 40 µl 3-(trimethoxysilyl) propylmethacrylate (Sigma Aldrich), 60 µl of glacial acetic acid diluted 1:10 in deionized (DI) water, and 1.9 ml of 100% ethanol. The coverslips were treated for approximately 15-20 minutes, washed with 100% ethanol, and dried using airflow. These were then placed in 60°C oven for about 30 minutes before use.

Next, polyacrylamide (PAm) gels were formed on each coverslip. Accordingly, 6.25 µl of 40% acrylamide solution, 5.625 µl of 2% bis-acrylamide solution, and 0.5 µl of 200 nm far red fluorescent particles were added to 38.1 µl PBS. A 10% ammonium persulfate (APS) and *N,N,N′,N′*-tetramethylethylenediamine (TEMED) solutions were prepared. 0.6 µl of each APS and TEMED solutions were added to the polyacrylamide solution and vortexed. 3 µl of this solution was added to the methacrylated 24x50 mm coverslip, and a non-treated 12 mm coverslip was added over the droplet. Similarly, a 3 µl droplet was added onto a non-treated coverslip and the methacrylated 12 mm coverslip was add. After about 30 minutes to allow polymerization, the gels were submerged in DI water and the coverslips were detached. This resulted in PAm gel on the methacrylated 24x50 mm coverslip and another gel on the methacrylated 12 mm coverslip.

A 5 µl Milli-Q water droplet was added on the chamber part of the silicon wafer, and the methacrylated 12 mm coverslip with PAm gel was added over the droplet, such

that the gel was in contact with the water. Next, a 10:1 polydimethylsiloxane (PDMS):curing agent mixture was thoroughly mixed, degassed, carefully poured over the wafer, and then cured at 60˚C. During this process, the coverslip becomes attached to the PDMS. The completed PDMS structure was cut and peeled from the wafer, and this results in a PDMS structure with the flow channels and the chamber containing the exposed PAm gel. To the complete the chip fabrication, the PDMS and the methacrylated glass, both with PAm gels, were exposed to UV-Ozone for 5 minutes and then bonded. This structure was allowed to completely bond in 60˚C oven.

3.3.4 Encapsulation of MCF-7 in GelMA inside Microfluidics Device

Prior to encapsulating cells inside, the device was perfused with PBS and sterilized using UV exposure. GelMA was weighed and dissolved in PBS to make 8% (w/v) solution, and kept in 60 ˚C until completely dissolved. The solution was then filtered to allow for sterile, long term cell culture. To prepare the cells for suspension in GelMA, the MCF7 spheroids were filtered through 40 μm cell filters, and spheroids mostly larger than 40 μm were collected and centrifuged at 500 rpm for 5 minutes. The spheroid pellet was resuspended in the 8% GelMA solution, and addition of fluorescent particles, LAP, and ascorbic acid yielded a solution composed of spheroids, 1% fluorescent particles, 2 mM LAP, and 0.01% ascorbic acid. This solution was introduced into the device, and exposed to microscope UV light through a photomask consisting of 320 μm circular pattern. Positioning of the pattern under spheroids of choice allowed for selective polymerization of GelMA to encapsulate specific spheroids. Next, 5%

penicillin-streptomycin in PBS solution was perfused to wash out excess spheroids and unpolymerized GelMA.

A 10 mL syringe containing growth media was connected using tubing to the inlet port of the device, while the outlet port was connected to a tubing with needle. The needle was connected to a stopcock valve. The 10 mL syringe was mounted onto a syringe pump, and the device was placed in a 37˚C and 10% CO_2 incubator. While in the incubator, the stopcock valve was set to the open position to allow flow of the growth media through the device for normal cell culture.

3.3.5 Compression Experiment

For the experiment, the device was removed from the incubator, and the syringe was removed from the pump. The valve at the outlet port of the device was closed while the syringe was kept at an approximate level of the chip itself. The device was then mounted on a Spinning Disk microscope with oil objective lens of 40x. The imaging was set to capture 3x3 fields of view with 15% overlap and stitched to generate a complete view of the XY image. This way, the bright field images of each sample was captured. In addition, to capture a 3D section of the fluorescent particles, for each sample within the device chamber, an arbitrary middle slice was chosen, and imaging was set to capture Z-slices 10 μm above and below this middle section at Z-increments of 0.2 μm.

To start the experiment, the syringe was placed next to the device, representing a relative height of 0 inches, and consequently, zero relative pressure. The syringe was maintained at that height for at least 15 minutes before imaging. Samples were identified

within a single device chamber. At this relative 0 pressure, the 3D stack for each sample was captured. Next, the syringe was moved to the relative height of approximately 11.5 inches, representing a relative pressure change of approximately 2.8 kPa, based on the hydrostatic expression, ρgh. Here, the density was of the growth media which was approximated to equal that of water. For the new pressure, the approximate middle z-slice for each sample was re-identified based on distinct beads distribution. This change was maintained for at least 15 minutes before imaging was resumed. These were repeated on Day 1, 2, 3, and 6.

3.3.6 Initial Image Processing

Before quantification of the displacements of the fluorescent particles due to the applied pressure, the overall XYZ image shift between the 3D stack at the two different pressures was identified. For this, the two different stacks were visualized using ImageJ, and by eye, mid-slices for the two stacks were matched based on similar beads distribution. From these matched mid-slices, 5 μm above and below the mid-slices were identified for further processing. This way, the Z shift was approximated and corrected visually. Next, these mid-slices were processed through MATLAB to identify XY shifts in the fields of view of the two images based on shifts in the centroids. These XY shift values were entered into the particle image velocimetry (PIV) algorithm.

3.3.7 Particle Image Velocimetry (PIV)

PIV interrogation box sizes in the x, y, and z dimensions were prescribed to be 100x100x15, with the shifts of 25x25x5. The displacements obtained from PIV were

converted to volumetric strains, first using the gradient function to obtain strains and then summing the normal strains.

3.3.8 Simulation

COMSOL was used to simulate pressure application on a cylindrical structure with dimensions of 320 μm in diameter and 120 μm in height. The cylindrical model was prescirbed to have homogeneous mechanical properties. For the boundary conditions, the applied pressure on the cylinder side was 2800 Pa, and the displacements at the top and bottom was set at 2 μm and 4 μm. The asymmetric displacement was used because of the potential asymmetric extension in the experimental condition. This simulation volumetric strain result was used as a means to identify the natural spatial variation in volumetric strains in the case of a sample with homogeneous material properties, and to identify the possible heterogeneity present in the hydrogel.

3.3.9 Analysis Methodology

The simulation yielded a theoretical volumetric strain. To calculate the volumetric strain deviation for each day, a single slice of empirical volumetric strain for a day was subtracted by the theoretical, and this was divided by the theoretical strain. In order to determine the changes relative to Day 1, the volumetric strain deviations for Days 2, 3, and 6 were resized to match the dimension of the Day 1 result. The volumetric strain deviations for Days 2, 3, and 6 were normalized to Day 1. This normalization was done by subtracting either Day 2, 3, or 6 strain deviation by the Day 1 deviation, and dividing the values by the Day 1 deviation. This normalizing to Day 1 approach allows

using a standard theoretical volumetric strain field, without requiring the simulation of the exact experimental hydrogel conditions, as long as there is no comparing across different sample conditions. Positive deviation, indicated possible stiffening of the material. Negative values indicated potential softening of the material. These connections between the strains and the changes in mechanical properties can be made under the assumption that the compression of the material was dominant, and any extension in the z direction of the block was negligible.

3.4 Results

3.4.1 Compression Method

This novel approach to determine possible changes in ECM mechanical properties utilizes the previously described photopatterning approach in conjunction with the application of hydrostatic pressure within a microfluidics device. The schematic in Figure 3.1 demonstrates the overall approach taken to apply a load onto the hydrogel. Raising the syringe, with the valve in closed position, introduces hydrostatic pressure within the device chamber and deforms the hydrogel. The deformations present include compression along the radial direction of the cylindrical structure and extension along the axial direction.

As seen in Figure 3.2A, the fluorescent particles were visualized using Spinning Disk microscope, and the cylindrical shape can be observed through the circular XY image and a height of approximately 80 μm. This sample was processed using PIV algorithm to determine the displacements and ultimately the volumetric strains, shown

in top Figure 3.2B. The presence of extension in the Z-direction, shown in the bottom part of Figure 3.2B was an indication that the deformation due to hydrostatic pressure was not entirely compression, but in fact there was certain chamber expansion, pulling on the samples in Z-direction when the pressure was increased.

As a first step, the simulation model, depicted in Figure 3.2C, consisted of a cylinder with height of 120 μm, with total extension percentage of 0.5%. The simulation used top displacement of 2 μm and bottom displacement of 4 μm. The reason for this asymmetric displacement assumption was the presence of PDMS layer above the chamber, but no such thick layer at the bottom. Next, the simulation result was compared to the experimental result (Figure 3.2D). An interesting aspect of the experimental result is the trend in volumetric strain where the compression is higher in the interior relative to the outer edge of the hydrogel. One of the reasons for this observation could be due to the photopolymerization process, where the light diffraction at the edges of the transparency pattern could yield more cross-linking. On the other hand, a possibility is that the box sizes used during PIV analysis may yield less accurate results at the edge because of very high displacements that may not be completely captured during the analysis.

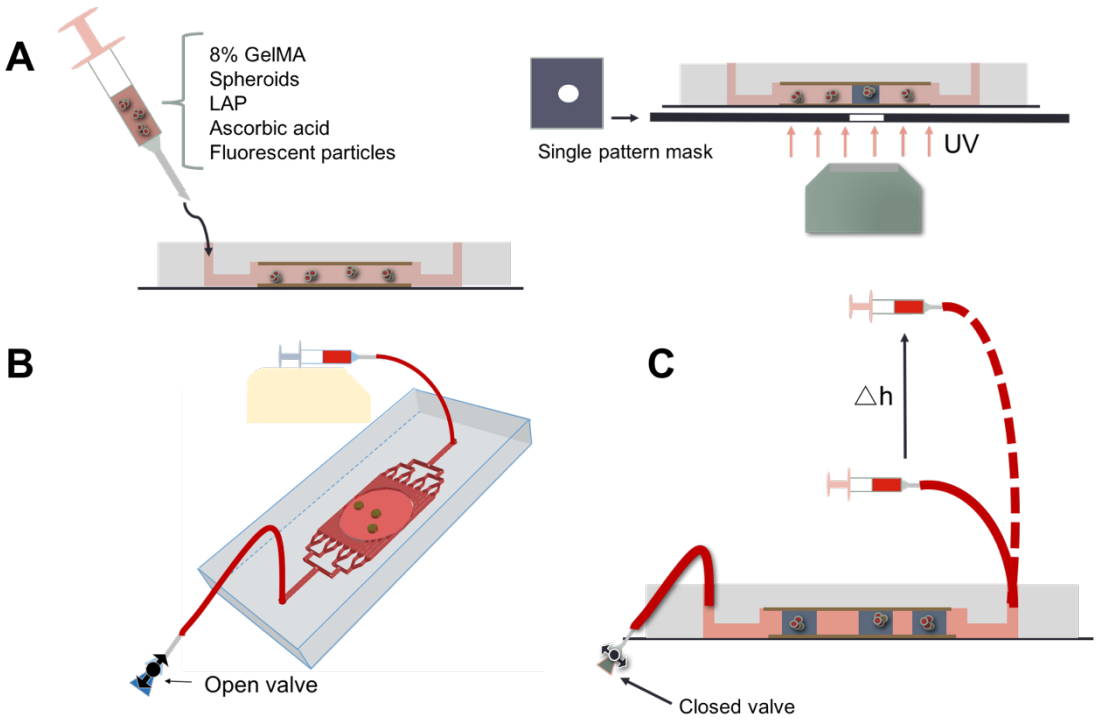

Figure 3.1. Schematic representation of the protocol for performing compression test on cell-laden GelMA structures. (A) Spheroids are suspended in the GelMA solution, supplemented with fluorescent particles, lithiumphenyl-2,4,6-trimethylbenoylphosphinate (LAP), and ascorbic acid. The solution is perfused through the microfluidic device. The device is exposed to UV through a photomask with specific pattern to form hydrogel structures with embedded spheroids. (B) The output tubing of the device is connected to a valve, which is set to open position for perfusion of growth media. (C) During the compression test, conducted at different timepoints, the valve is closed, and an open syringe is connected to the input. To apply hydrostatic pressure, the syringe height is varied. The hydrogel structure is imaged when the syringe is at two different heights to detect the compression of the hydrogel due to pressure.

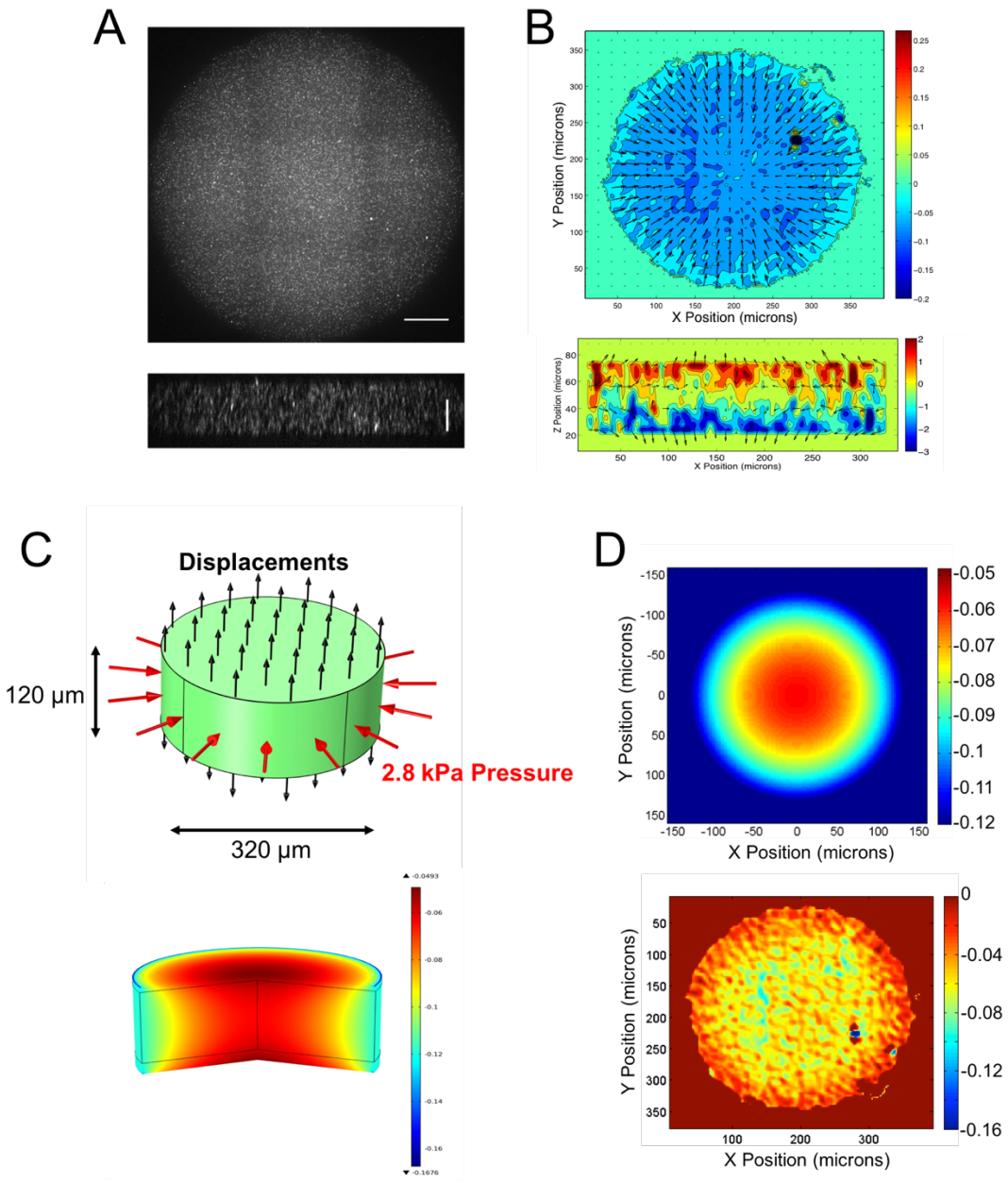

Figure 3.2. Acellular constructs were visualized using fluorescent beads, and the deformations were determined using particle image velocimetry (PIV). (A) An XY view of the cylindrical hydrogel structure (top) and a cross-section view XZ of the structure (bottom). Horizontal scale bar: 50 µm. Vertical scale bar: 50 µm. **(**B) PIV was used to obtain the displacement field in three-dimensions. Volumetric strain was calculated from the displacement field. The top color map represents the volumetric strain, and the arrows indicate the displacements (top). The bottom color map represents the vertical displacements and arrows represent the displacement field of this acellular sample (bottom). (C) Simulation of cylinder with prescribed boundary conditions (top) and a simulated volumetric strain field (bottom). (D) A cross-section simulated volumetric strain (top) and an experimental volumetric strain (bottom).

3.4.2 Simulation Results

In an effort to understand the relationship between the volumetric strain changes and mechanical properties of the structure, simulations were run for varying bulk modulus (B) and shear modulus (G). For arbitrary baseline moduli the volumetric strains were determined, and as a function of radius are represented in the black curve in Figure 3.3A. Lowering the bulk modulus (B) resulted in more negative volumetric strain, and increasing the bulk modulus yielded less negative volumetric strain. The divergence from the baseline is greater with increasing radius. The shear modulus on the other hand tended to converge towards the baseline with increasing radius. Figures 3.3B and 3.3C demonstrate that the volumetric strain deviations from the baseline, are dependent on both the bulk (K) and shear modulus (G), closer to the center of the structure, as seen by the non-zero mean values in Figure 3.3B. However, the shear modulus affect tends towards zero with increasing radius. Based on these simulation results seen in Figure 3.3, as the radius increases, there is a trend toward increasing bulk modulus dependence on the volumetric strain. Additionally, the color maps indicate that when the bulk and shear modulus change are positive, the volumetric strain deviation percentage also tends to be positive. Similarly, when bulk and shear modulus deviation are negative, the deviation in volumetric strain also tends to be negative.

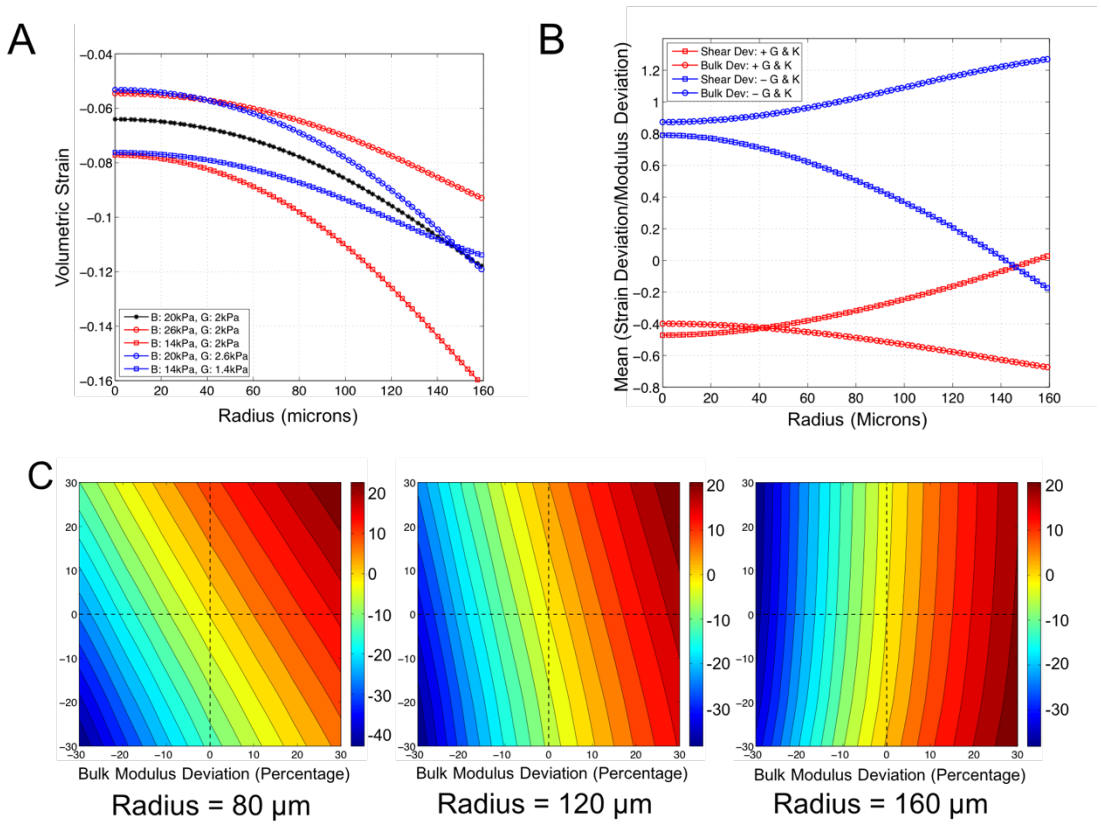

Figure 3.3: Determining the effects of deviations in shear modulus and bulk modulus on the volumetric strains deviations for different radial positions. (A) The volumetric strains as a function of cylinder radial position was plotted for different bulk moduli, *B*, and shear moduli, *G*. (B) Mean values of the ratio of deviation in volumetric strain to modulus deviation, as a function of radius. (C) The percentage deviation of volumetric strains is represented by the color maps as a function of bulk modulus (horizontal axis) and shear modulus deviation (vertical axis).

3.4.3 Spheroid Growth and Changes in Matrix Properties

As seen in the top row of Figure 3.4A, a spheroid encapsulated on Day 0 within a GelMA hydrogel, inside a microfluidics chamber, was observed to grow through Day 6. The overall growth in size was also observed in the fluorescent particles images by the increase in the size of the interior region lacking the particles, representing the space where a spheroid was present. In addition to the increase in the interior area, the overall

area of the hydrogel also increased, through outward expansion. Next, the deviation of volumetric strains, relative to the theoretical values were quantified for each day. The Day 1 in Figure 3.4B is a representation of this deviation quantification. These volumetric strain deviation quantities for Days 2, 3, and 6 were further normalized to Day 1, shown in the remaining 3 maps in Figure 3.4B. Recognizing that the overall area of the hydrogel outline increased with days, before the normalization, each Day sample was resized through image processing to fit the size of the Day 1 sample.

The overall deviation, both negative and positive combined, was quantified as a function of radius starting with the spheroid periphery. When deviation values only greater than +1 and less than -1 were combined for different normalized radial values, results indicated that there was overall greater deviation closer to the spheroids, and these decreased farther away (Figure 3.4C). Next, positive and negative normalized deviation was determined. Specifically, the radii range that contained high number of total deviation was considered, and values less than -1 and greater than 1 were further categorized as negative or positive. Results averaged from 3 different samples demonstrated positive deviation was prominent on all days, possibly indicating consistent stiffening. This could be a result of pushing on the GelMA material as a result of spheroid growth. The difference between -1 and +1 deviation categories appears greater for Day 6, compared to Day 2 and 3. Another interesting note is the lack of significant increase in the positive deviation on Day 6, compared to Day 2.

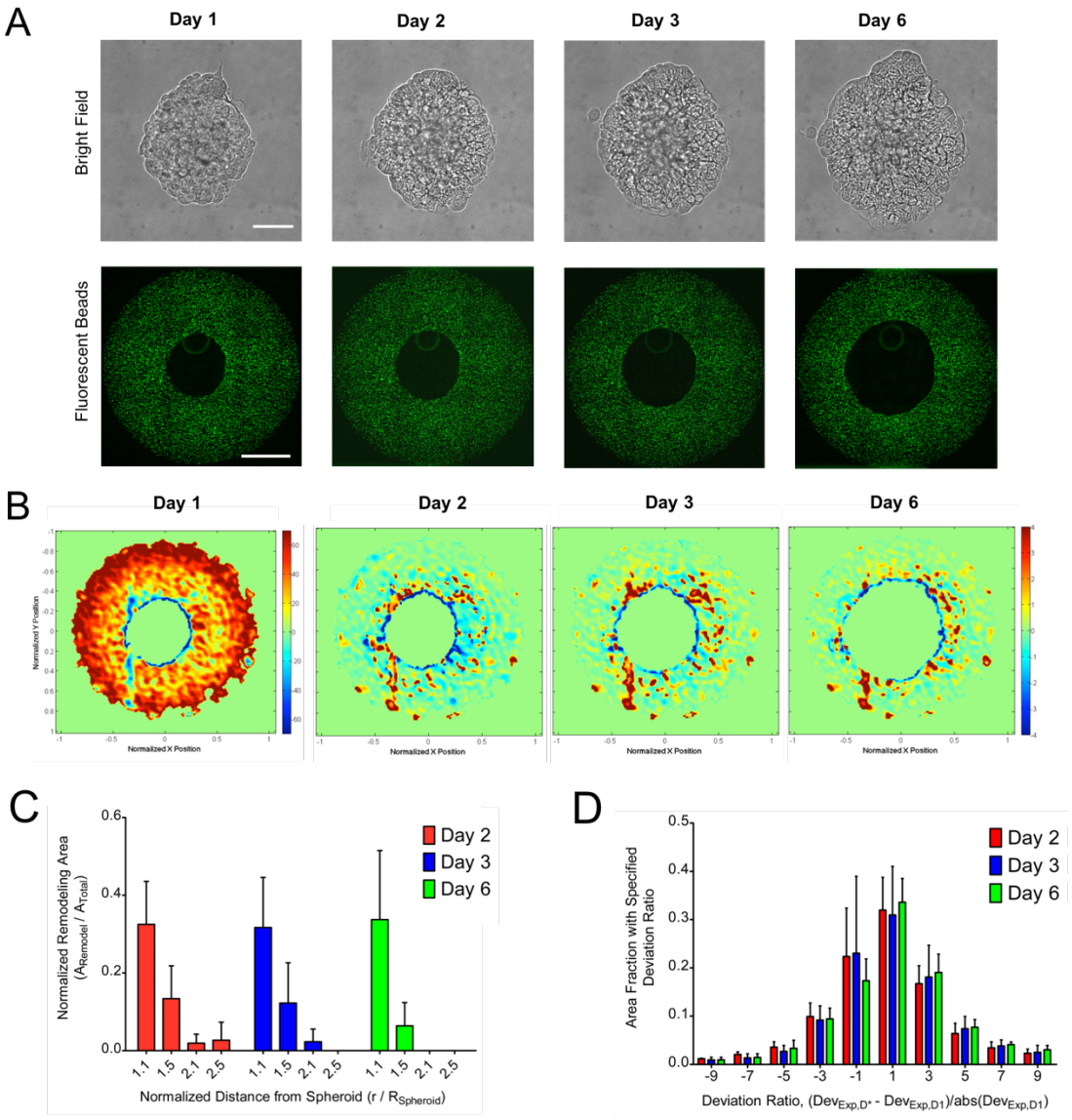

Figure 3.4. Cell proliferation and dynamic matrix mechanical properties. (A) Spheroid growth as a function culture time, from Day 1 post-encapsulation through Day 6 (top). For the bright field images, scale bar: 50 µm. A set of fluorescent particles around a spheroid for different days of growth (bottom). The green indicates the fluorescent particles embedded within the GelMA structure. For the fluorescence images, scale bar: 100 µm. (B) Deviation in volumetric strain for Day 1 relative to simulated results is represented as percent deviation. Days 2, 3, and 6 were normalized to Day 1 results. (C) Deviation ratio greater than 1 or less than -1 was used for quantification. The area of deviation, or the total number of deviation values than are greater 1 or less than 1 combined, and that fall within than normalized radial value, normalized to total area of a normalized radial value, shows overall deviation close to and farther from the spheroid periphery. (D) The distribution of deviation ratio for different days of culture indicate the possible changes in matrix properties occurring around growing spheroids.

3.5 Discussion and Future Directions

We aimed to extend the photopatterning approach to study cancer growth and quantify any associated changes in matrix mechanical properties. We introduced the microfluidics aspect to allow for a flow system, which can then be used as a tool to provide hydrostatic pressures to the system. Here, we injected spheroid-GelMA solution into the microfluidic device, exposed to UV through a photomask, and generated cylindrical structures, with a spheroid in the interior. These samples were perfused with media, and thus a culture system was generated. Introduction of relative hydrostatic pressure, through change of height resulted in the deformation of the hydrogel structure, through compression in the transverse plane (X-Y plane), and extension in the axial (Z plane). The extension was likely a result of the chamber expansion through glass bending.

In the experiments involving cell growth and monitoring over time, the relative volumetric strain deviations were determined by comparing the deviation from theoretical result for different days to Day 1 deviation result. These relative deviations were classified as positive or negative. In a system where compression dominates, and the extension is negligible, after hydrostatic pressure application, the negative deviations can be attributed to possible softening of the material, and positive deviations can be attributed to possible stiffening of the material. In the experimental case with cells, the PIV output for a given hydrogel section suggested that the extension appeared to be relatively small compared to the compression. This could be because of the overall small thin section that was imaged and analyzed, limiting the extent of extension influence. Additionally, another important factor that could contribute to the lower extension strain

values are the PIV parameters used during displacement calculation. The interrogation box size chosen for the z direction may have not completely captured the beads displacement. This suggests that optimization of the interrogation box size is a critical step. This can be done in future experiments by performing the compression experiment on multiple acellular samples and capturing thicker sections. By visually determining displacements of the beads, and running the images through PIV using several interrogation box sizes, one can aim to obtain box sizes that correctly capture the displacement. Nevertheless, in order to correctly connect the volumetric strains to the mechanical properties, the extension has to be negligible compared to the compression. This requirement can be addressed in the future by attempting to minimize the extension through use of different hydrogel geometry, like taller structures, or using thicker glass slices for microfluidics device fabrication to minimize bending. The drawback of this is that the thicker glass will prevent higher magnification imaging, thus compromising resolution. On the other hand, using lower magnification would reduce the potential of having stitching artifact present in the images because using higher magnification imaging requires stitching different fields of view to capture the entire hydrogel sample in the XY dimension.

Other improvement needed for the system include use of an open syringe during compression application. The previously described experiments were conducted with a regular closed syringe, with the liquid not exposed to the atmosphere. The pressure application was performed by changing the height of the syringe in a horizontal position. Therefore, the liquid volume in the syringe itself does not play a role. However, in the open syringe, the syringe can be placed in a vertical direction with the liquid column

inside affecting the hydrostatic pressure. Changing the height of this open syringe will result in a pressure change causing deformation of the hydrogel. With this set up, the liquid column height is important because in the vertical position, the liquid height will determine the initial state of the hydrogel at relative zero pressure. This liquid and syringe height, and therefore the initial state has to be as consistent as possible for different days so that the comparisons relative to Day 1 can be accurately performed. Then, a direct translation of the syringe will cause increase in hydrostatic pressure, and keeping this height change consistent can ensure similar pressure application every day. Additionally, overall automation of the compression testing and image processing and analysis will further improve the consistency of the results.

Overall, this was a proof-of-concept of a novel method to assess changes in the mechanical properties by applying a load and detecting a deformation within an in vitro system. For this, we characterized one method of pressure application and resulting hydrogel deformation detection. The volumetric strain calculation process and important improvements associated with these calculations, and the possible simulation and image processing-based analysis method were described. Finally, the ability to determine the changes in the mechanical properties of the matrix based on volumetric strain deviations using this method was deemed to be dependent on negligible extension of the overall hydrogel deformation. This last aspect, considering our samples had overall hydrogel extension, would require making significant adjustments to the current set up, such as hydrogel geometry and thicker glass coverslips used for device fabrication.

3.6 Acknowledgements

Chapter 3, in full, is a result of collaborative work with Aereas Aung. The author also acknowledges Professor Juan Carlos del Alamo and his research group for the Particle Image Velocimetry MATLAB algorithm. Finally, the author acknowledges Jomkuan Theprungsirikul for guidance in microfluidics device preparation and help with cell encapsulation steps. The thesis author was a primary investigator and author of this chapter.

REFERENCES

1. Tibbitt MW, Anseth KS. Hydrogels as extracellular matrix mimics for 3D cell culture. Biotechnol. Bioeng. **103**(4), 655, 2009;

2. Daley WP, Peters SB, Larsen M. Extracellular matrix dynamics in development and regenerative medicine. J. Cell Sci. **121**(3), 255, 2008;

3. Bissell MJ, Kenny PA, Radisky DC. Microenvironmental regulators of tissue structure and function also regulate tumor induction and progression: the role of extracellular matrix and its degrading enzymes. Cold Spring Harb. Symp. Quant. Biol. **70**, 343, 2005;

4. Cox TR, Erler JT. Remodeling and homeostasis of the extracellular matrix: implications for fibrotic diseases and cancer. Dis. Model. Mech. **4**(2), 165, 2011;

5. Lu P, Takai K, Weaver VM, Werb Z. Extracellular Matrix Degradation and Remodeling in Development and Disease. Cold Spring Harb. Perspect. Biol. **3**(12), a005058, 2011;

6. Hutmacher DW, Horch RE, Loessner D, Rizzi S, Sieh S, Reichert JC, Clements JA, Beier JP, Arkudas A, Bleiziffer O, Kneser U. Translating tissue engineering technology platforms into cancer research. J. Cell. Mol. Med. **13**(8a), 1417, 2009;

7. Saha K, Pollock JF, Schaffer DV, Healy KE. Designing synthetic materials to control stem cell phenotype. Curr. Opin. Chem. Biol. **11**(4), 381, 2007;

8. Hutmacher DW. Biomaterials offer cancer research the third dimension. Nat. Mater. **9**(2), 90, 2010;

9. Siegel RL, Miller KD, Jemal A. Cancer statistics, 2016. CA. Cancer J. Clin. **66**(1), 7, 2016;

10. Torre LA, Bray F, Siegel RL, Ferlay J, Lortet-Tieulent J, Jemal A. Global cancer statistics, 2012. CA. Cancer J. Clin. **65**(2), 87, 2015;

11. Khetan S, Burdick JA. Patterning hydrogels in three dimensions towards controlling cellular interactions. Soft Matter. **7**(3), 830, 2011;

12. Yanagawa F, Sugiura S, Kanamori T. Hydrogel microfabrication technology toward three dimensional tissue engineering. Regen. Ther. **3**, 45, 2016;

13. Bloom RJ, George JP, Celedon A, Sun SX, Wirtz D. Mapping Local Matrix Remodeling Induced by a Migrating Tumor Cell Using Three-Dimensional Multiple-Particle Tracking. Biophys. J. **95**(8), 4077, 2008;

14. Jones DP, Hanna W, El-Hamidi H, Celli JP. Longitudinal Measurement of Extracellular Matrix Rigidity in 3D Tumor Models Using Particle-tracking Microrheology. J. Vis. Exp. [Internet]. (88), 2014 [cited 2016 Sep 20]; Available from: http://www.jove.com/video/51302/longitudinal-measurement-extracellular-matrix-rigidity-3d-tumor

15. van Dijk M, Göransson SA, Strömblad S. Cell to extracellular matrix interactions and their reciprocal nature in cancer. Exp. Cell Res. **319**(11), 1663, 2013;

16. Barczyk M, Carracedo S, Gullberg D. Integrins. Cell Tissue Res. **339**(1), 269, 2010;

17. Askari JA, Buckley PA, Mould AP, Humphries MJ. Linking integrin conformation to function. J. Cell Sci. **122**(2), 165, 2009;

18. Giancotti FG, Ruoslahti E. Integrin signaling. Science. **285**(5430), 1028, 1999;

19. Wang N, Tytell JD, Ingber DE. Mechanotransduction at a distance: mechanically coupling the extracellular matrix with the nucleus. Nat. Rev. Mol. Cell Biol. **10**(1), 75, 2009;

20. Maniotis AJ, Chen CS, Ingber DE. Demonstration of mechanical connections between integrins, cytoskeletal filaments, and nucleoplasm that stabilize nuclear structure. Proc. Natl. Acad. Sci. U. S. A. **94**(3), 849, 1997;

21. Streuli CH. Integrins as architects of cell behavior. Mol. Biol. Cell. **27**(19), 2885, 2016;

22. Ranga A, Lutolf MP. High-throughput approaches for the analysis of extrinsic regulators of stem cell fate. Curr. Opin. Cell Biol. **24**(2), 236, 2012;

23. Rape AD, Zibinsky M, Murthy N, Kumar S. A synthetic hydrogel for the high-throughput study of cell–ECM interactions. Nat. Commun. **6**, 8129, 2015;

24. Mabry KM, Schroeder ME, Payne SZ, Anseth KS. Three-Dimensional High-Throughput Cell Encapsulation Platform to Study Changes in Cell-Matrix Interactions. ACS Appl. Mater. Interfaces. **8**(34), 21914, 2016;

25. Lu P, Weaver VM, Werb Z. The extracellular matrix: A dynamic niche in cancer progression. J. Cell Biol. **196**(4), 395, 2012;

26. Ao M, Brewer BM, Yang L, Franco Coronel OE, Hayward SW, Webb DJ, Li D. Stretching Fibroblasts Remodels Fibronectin and Alters Cancer Cell Migration. Sci. Rep. **5**, 8334, 2015;

27. Fraley SI, Wu P, He L, Feng Y, Krisnamurthy R, Longmore GD, Wirtz D. Three-dimensional matrix fiber alignment modulates cell migration and MT1-MMP utility by spatially and temporally directing protrusions. Sci. Rep. **5**, 14580, 2015;

28. Gattazzo F, Urciuolo A, Bonaldo P. Extracellular matrix: A dynamic microenvironment for stem cell niche. Biochim. Biophys. Acta BBA - Gen. Subj. **1840**(8), 2506, 2014;

29. Paluch EK, Nelson CM, Biais N, Fabry B, Moeller J, Pruitt BL, Wollnik C, Kudryasheva G, Rehfeldt F, Federle W. Mechanotransduction: use the force(s). BMC Biol. [Internet]. **13**(1), 2015 [cited 2016 Sep 21]; Available from: http://www.biomedcentral.com/1741-7007/13/47

30. Egeblad M, Werb Z. New functions for the matrix metalloproteinases in cancer progression. Nat. Rev. Cancer. **2**(3), 161, 2002;

31. Page-McCaw A, Ewald AJ, Werb Z. Matrix metalloproteinases and the regulation of tissue remodelling. Nat. Rev. Mol. Cell Biol. **8**(3), 221, 2007;

32. Levental KR, Yu H, Kass L, Lakins JN, Egeblad M, Erler JT, Fong SFT, Csiszar K, Giaccia A, Weninger W, Yamauchi M, Gasser DL, Weaver VM. Matrix Crosslinking Forces Tumor Progression by Enhancing Integrin Signaling. Cell. **139**(5), 891, 2009;

33. Malik R, Lelkes PI, Cukierman E. Biomechanical and biochemical remodeling of stromal extracellular matrix in cancer. Trends Biotechnol. **33**(4), 230, 2015;

34. Birgersdotter A, Sandberg R, Ernberg I. Gene expression perturbation in vitro—A growing case for three-dimensional (3D) culture systems. Semin. Cancer Biol. **15**(5), 405, 2005;

35. Petersen OW, Rønnov-Jessen L, Howlett AR, Bissell MJ. Interaction with basement membrane serves to rapidly distinguish growth and differentiation pattern of normal and malignant human breast epithelial cells. Proc. Natl. Acad. Sci. U. S. A. **89**(19), 9064, 1992;

36. Kim JB, Stein R, O'Hare MJ. Three-dimensional in vitro tissue culture models of breast cancer — a review. Breast Cancer Res. Treat. **85**(3), 281.

37. Xu G, Yin F, Wu H, Hu X, Zheng L, Zhao J. In vitro ovarian cancer model based on three-dimensional agarose hydrogel. J. Tissue Eng. [Internet]. **5**(0), 2014 [cited 2016 Sep 22]; Available from: http://tej.sagepub.com/lookup/doi/10.1177/2041731413520438

38. Kaji H, Camci-Unal G, Langer R, Khademhosseini A. Engineering systems for the generation of patterned co-cultures for controlling cell-cell interactions. Biochim. Biophys. Acta. **1810**(3), 239, 2011;

39. Underhill GH, Chen AA, Albrecht DR, Bhatia SN. Assessment of hepatocellular function within PEG hydrogels. Biomaterials. **28**(2), 256, 2007;

40. Ehsan SM, Welch-Reardon KM, Waterman ML, Hughes CCW, George SC. A three-dimensional in vitro model of tumor cell intravasation. Integr. Biol. **6**(6), 603, 2014;

41. Lee KY, Mooney DJ. Hydrogels for Tissue Engineering. Chem. Rev. **101**(7), 1869, 2001;

42. Caliari SR, Burdick JA. A practical guide to hydrogels for cell culture. Nat. Methods. **13**(5), 405, 2016;

43. Yang Y, Motte S, Kaufman LJ. Pore size variable type I collagen gels and their interaction with glioma cells. Biomaterials. **31**(21), 5678, 2010;

44. Aung A, Seo YN, Lu S, Wang Y, Jamora C, del Álamo JC, Varghese S. 3D Traction Stresses Activate Protease-Dependent Invasion of Cancer Cells. Biophys. J. **107**(11), 2528, 2014;

45. Caliari SR, Perepelyuk M, Cosgrove BD, Tsai SJ, Lee GY, Mauck RL, Wells RG, Burdick JA. Stiffening hydrogels for investigating the dynamics of hepatic stellate cell mechanotransduction during myofibroblast activation. Sci. Rep. **6**, 21387, 2016;

46. Sala A, Hänseler P, Ranga A, Lutolf MP, Vörös J, Ehrbar M, Weber FE. Engineering 3D cell instructive microenvironments by rational assembly of artificial extracellular matrices and cell patterning. Integr. Biol. **3**(11), 1102, 2011;

47. Guvendiren M, Perepelyuk M, Wells RG, Burdick JA. Hydrogels with differential and patterned mechanics to study stiffness-mediated myofibroblastic differentiation of hepatic stellate cells. J. Mech. Behav. Biomed. Mater. **38**, 198, 2014;

48. Hanjaya-Putra D, Wong KT, Hirotsu K, Khetan S, Burdick JA, Gerecht S. Spatial control of cell-mediated degradation to regulate vasculogenesis and angiogenesis in hyaluronan hydrogels. Biomaterials. **33**(26), 6123, 2012;

49. Stevens KR, Miller JS, Blakely BL, Chen CS, Bhatia SN. Degradable hydrogels derived from PEG-diacrylamide for hepatic tissue engineering. J. Biomed. Mater. Res. A. **103**(10), 3331, 2015;

50. Cuchiara ML, Coşkun S, Banda OA, Horter KL, Hirschi KK, West JL. Bioactive poly(ethylene glycol) hydrogels to recapitulate the HSC niche and facilitate HSC expansion in culture. Biotechnol. Bioeng. **113**(4), 870, 2016;

51. Benton JA, DeForest CA, Vivekanandan V, Anseth KS. Photocrosslinking of Gelatin Macromers to Synthesize Porous Hydrogels That Promote Valvular Interstitial Cell Function. Tissue Eng. Part A. **15**(11), 3221, 2009;

52. Zorlutuna P, Annabi N, Camci-Unal G, Nikkhah M, Cha JM, Nichol JW, Manbachi A, Bae H, Chen S, Khademhosseini A. Microfabricated Biomaterials for Engineering 3D Tissues. Adv. Mater. **24**(14), 1782, 2012;

53. Kolesky DB, Truby RL, Gladman AS, Busbee TA, Homan KA, Lewis JA. 3D Bioprinting of Vascularized, Heterogeneous Cell-Laden Tissue Constructs. Adv. Mater. **26**(19), 3124, 2014;

54. Nichol JW, Koshy ST, Bae H, Hwang CM, Yamanlar S, Khademhosseini A. Cell-laden microengineered gelatin methacrylate hydrogels. Biomaterials. **31**(21), 5536, 2010;

55. Liu VA, Bhatia SN. Three-Dimensional Photopatterning of Hydrogels Containing Living Cells. Biomed. Microdevices. **4**(4), 257.

56. Hammoudi TM, Lu H, Temenoff JS. Long-Term Spatially Defined Coculture Within Three-Dimensional Photopatterned Hydrogels. Tissue Eng. Part C Methods. **16**(6), 1621, 2010;

57. Billiet T, Vandenhaute M, Schelfhout J, Van Vlierberghe S, Dubruel P. A review of trends and limitations in hydrogel-rapid prototyping for tissue engineering. Biomaterials. **33**(26), 6020, 2012;

58. Stanton MM, Samitier J, Sánchez S. Bioprinting of 3D hydrogels. Lab. Chip. **15**(15), 3111, 2015;

59. Kumar S, Weaver VM. Mechanics, malignancy, and metastasis: The force journey of a tumor cell. Cancer Metastasis Rev. **28**(1–2), 113, 2009;

60. Tlsty TD, Coussens LM. Tumor Stroma and Regulation of Cancer Development. Annu. Rev. Pathol. Mech. Dis. **1**(1), 119, 2006;

61. Quail DF, Joyce JA. Microenvironmental regulation of tumor progression and metastasis. Nat. Med. **19**(11), 1423, 2013;

62. Cooper GM. The Development and Causes of Cancer. 2000 [cited 2016 Sep 26]; Available from: https://www.ncbi.nlm.nih.gov/books/NBK9963/

63. Norbury CJ, Zhivotovsky B. DNA damage-induced apoptosis. Oncogene. **23**(16), 2797, 2004;

64. Lowe SW, Lin AW. Apoptosis in cancer. Carcinogenesis. **21**(3), 485, 2000;

65. Yu H, Mouw JK, Weaver VM. Forcing form and function: biomechanical regulation of tumor evolution. Trends Cell Biol. **21**(1), 47, 2011;

66. Lorusso G, Rüegg C. The tumor microenvironment and its contribution to tumor evolution toward metastasis. Histochem. Cell Biol. **130**(6), 1091, 2008;

67. Cheng G, Tse J, Jain RK, Munn LL. Micro-Environmental Mechanical Stress Controls Tumor Spheroid Size and Morphology by Suppressing Proliferation and Inducing Apoptosis in Cancer Cells. PLOS ONE. **4**(2), e4632, 2009;

68. Alessandri K, Sarangi BR, Gurchenkov VV, Sinha B, Kießling TR, Fetler L, Rico F, Scheuring S, Lamaze C, Simon A, Geraldo S, Vignjevic D, Domejean H, Rolland L, Funfak A, Bibette J, Bremond N, Nassoy P. Cellular capsules as a tool for multicellular spheroid production and for investigating the mechanics of tumor progression in vitro. Proc. Natl. Acad. Sci. **110**(37), 14843, 2013;

69. Schedin P, Keely PJ. Mammary Gland ECM Remodeling, Stiffness, and Mechanosignaling in Normal Development and Tumor Progression. Cold Spring Harb. Perspect. Biol. **3**(1), a003228, 2011;

70. Wang K, Andresen Eguiluz RC, Wu F, Seo BR, Fischbach C, Gourdon D. Stiffening and unfolding of early deposited-fibronectin increase proangiogenic factor secretion by breast cancer-associated stromal cells. Biomaterials. **54**, 63, 2015;

71. Gennisson J-L, Deffieux T, Fink M, Tanter M. Ultrasound elastography: Principles and techniques. Diagn. Interv. Imaging. **94**(5), 487, 2013;

72. Mariappan YK, Glaser KJ, Ehman RL. MAGNETIC RESONANCE ELASTOGRAPHY: A REVIEW. Clin. Anat. N. Y. N. **23**(5), 497, 2010;

73. Ophir J, Céspedes I, Ponnekanti H, Yazdi Y, Li X. Elastography: A quantitative method for imaging the elasticity of biological tissues. Ultrason. Imaging. **13**(2), 111, 1991;

74. Itoh A, Ueno E, Tohno E, Kamma H, Takahashi H, Shiina T, Yamakawa M, Matsumura T. Breast Disease: Clinical Application of US Elastography for Diagnosis. Radiology. **239**(2), 341, 2006;

75. Lopez JI, Kang I, You W-K, McDonald DM, Weaver VM. In situ force mapping of mammary gland transformation. Integr. Biol. **3**(9), 910, 2011;

76. Khatau SB, Bloom RJ, Bajpai S, Razafsky D, Zang S, Giri A, Wu P-H, Marchand J, Celedon A, Hale CM, Sun SX, Hodzic D, Wirtz D. The distinct roles of the nucleus and nucleus-cytoskeleton connections in three-dimensional cell migration. Sci. Rep. [Internet]. **2**, 2012 [cited 2016 Oct 21]; Available from: http://www.nature.com/articles/srep00488

77. Williams RM, Zipfel WR, Webb WW. Interpreting Second-Harmonic Generation Images of Collagen I Fibrils. Biophys. J. **88**(2), 1377, 2005;

78. Chen X, Nadiarynkh O, Plotnikov S, Campagnola PJ. Second harmonic generation microscopy for quantitative analysis of collagen fibrillar structure. Nat. Protoc. **7**(4), 654, 2012;

79. Franken PA, Hill AE, Peters CW, Weinreich G. Generation of Optical Harmonics. Phys. Rev. Lett. **7**(4), 118, 1961;

80. Campagnola PJ, Clark HA, Mohler WA, Lewis A, Loew LM. Second-harmonic imaging microscopy of living cells. J. Biomed. Opt. **6**(3), 277, 2001;

81. Gordon VD, Valentine MT, Gardel ML, Andor-Ardó D, Dennison S, Bogdanov AA, Weitz DA, Deisboeck TS. Measuring the mechanical stress induced by an expanding multicellular tumor system: a case study. Exp. Cell Res. **289**(1), 58, 2003;

82. Schultz KM, Anseth KS. Monitoring degradation of matrix metalloproteinases-cleavable PEG hydrogels via multiple particle tracking microrheology. Soft Matter. **9**(5), 1570, 2013;

83. Álamo JC del, Meili R, Álvarez-González B, Alonso-Latorre B, Bastounis E, Firtel R, Lasheras JC. Three-Dimensional Quantification of Cellular Traction Forces and Mechanosensing of Thin Substrata by Fourier Traction Force Microscopy. PLOS ONE. **8**(9), e69850, 2013;

84. Hsiao AY, Torisawa Y, Tung Y-C, Sud S, Taichman RS, Pienta KJ, Takayama S. Microfluidic system for formation of PC-3 prostate cancer co-culture spheroids. Biomaterials. **30**(16), 3020, 2009;

85. Ying L, Wang Q. Microfluidic chip-based technologies: emerging platforms for cancer diagnosis. BMC Biotechnol. **13**(1), 76, 2013;

86. Tien J, Li L, Ozsun O, Ekinci KL. Dynamics of Interstitial Fluid Pressure in Extracellular Matrix Hydrogels in Microfluidic Devices. J. Biomech. Eng. **137**(9), 2015;

87. Polacheck WJ, Charest JL, Kamm RD. Interstitial flow influences direction of tumor cell migration through competing mechanisms. Proc. Natl. Acad. Sci. **108**(27), 11115, 2011;

88. MacQueen L, Chebotarev O, Chen M, Usprech J, Sun Y, Simmons CA. Three-Dimensional Mechanical Compression of Biomaterials in a Microfabricated Bioreactor with On-Chip Strain Sensor. Okinawa, Japan; 2012.

89. Kao YC, Lee CH, Kuo PL. Increased hydrostatic pressure enhances motility of lung cancer cells. 2014 36th Annu. Int. Conf. IEEE Eng. Med. Biol. Soc. p. 2928–31, 2014.

90. Aung A, Theprungsirikul J, Lim HL, Varghese S. Chemotaxis-driven assembly of endothelial barrier in a tumor-on-a-chip platform. Lab. Chip. **16**(10), 1886, 2016;

91. Aung A, Bhullar IS, Theprungsirikul J, Davey SK, Lim HL, Chiu Y-J, Ma X, Dewan S, Lo Y-H, McCulloch A, Varghese S. 3D cardiac μtissues within a microfluidic device with real-time contractile stress readout. Lab. Chip. **16**(1), 153, 2015;

92. Ali S, Cuchiara ML, West JL. Chapter 8 - Micropatterning of Poly(ethylene glycol) Diacrylate Hydrogels. In: Théry MP and M, editor. Methods Cell Biol. [Internet]. Academic Press; p. 105–19, 2014 [cited 2016 Oct 5]. Available from: http://www.sciencedirect.com/science/article/pii/B9780128002810000087

93. Discher DE, Mooney DJ, Zandstra PW. Growth Factors, Matrices, and Forces Combine and Control Stem Cells. Science. **324**(5935), 1673, 2009;

94. Khetan S, Guvendiren M, Legant WR, Cohen DM, Chen CS, Burdick JA. Degradation-mediated cellular traction directs stem cell fate in covalently crosslinked three-dimensional hydrogels. Nat. Mater. **12**(5), 458, 2013;

95. Kang H, Shih Y-RV, Hwang Y, Wen C, Rao V, Seo T, Varghese S. Mineralized gelatin methacrylate-based matrices induce osteogenic differentiation of human induced pluripotent stem cells. Acta Biomater. **10**(12), 4961, 2014;

96. Benoit DSW, Schwartz MP, Durney AR, Anseth KS. Small functional groups for controlled differentiation of hydrogel-encapsulated human mesenchymal stem cells. Nat. Mater. **7**(10), 816, 2008;

97. Huebsch N, Arany PR, Mao AS, Shvartsman D, Ali OA, Bencherif SA, Rivera-Feliciano J, Mooney DJ. Harnessing traction-mediated manipulation of the cell/matrix interface to control stem-cell fate. Nat. Mater. **9**(6), 518, 2010;

98. Lim HL, Chuang JC, Tran T, Aung A, Arya G, Varghese S. Dynamic Electromechanical Hydrogel Matrices for Stem Cell Culture. Adv. Funct. Mater. **21**(1), 55, 2011;

99. Varghese S, Hwang NS, Ferran A, Hillel A, Theprungsirikul P, Canver AC, Zhang Z, Gearhart J, Elisseeff J. Engineering Musculoskeletal Tissues with Human Embryonic Germ Cell Derivatives. STEM CELLS. **28**(4), 765, 2010;

100. Mosiewicz KA, Kolb L, van der Vlies AJ, Martino MM, Lienemann PS, Hubbell JA, Ehrbar M, Lutolf MP. In situ cell manipulation through enzymatic hydrogel photopatterning. Nat. Mater. **12**(11), 1072, 2013;

101. Wade RJ, Bassin EJ, Gramlich WM, Burdick JA. Nanofibrous Hydrogels with Spatially Patterned Biochemical Signals to Control Cell Behavior. Adv. Mater. **27**(8), 1356, 2015;

102. Wylie RG, Ahsan S, Aizawa Y, Maxwell KL, Morshead CM, Shoichet MS. Spatially controlled simultaneous patterning of multiple growth factors in three-dimensional hydrogels. Nat. Mater. **10**(10), 799, 2011;

103. Liu Tsang V, Bhatia SN. Three-dimensional tissue fabrication. Adv. Drug Deliv. Rev. **56**(11), 1635, 2004;

104. Soman P, Chung PH, Zhang AP, Chen S. Digital microfabrication of user-defined 3D microstructures in cell-laden hydrogels. Biotechnol. Bioeng. **110**(11), 3038, 2013;

105. Khetan S, Burdick JA. Patterning network structure to spatially control cellular remodeling and stem cell fate within 3-dimensional hydrogels. Biomaterials. **31**(32), 8228, 2010;

106. Murphy SV, Atala A. 3D bioprinting of tissues and organs. Nat. Biotechnol. **32**(8), 773, 2014;

107. DeForest CA, Anseth KS. Cytocompatible click-based hydrogels with dynamically tunable properties through orthogonal photoconjugation and photocleavage reactions. Nat. Chem. **3**(12), 925, 2011;

108. Arcaute K, Mann BK, Wicker RB. Stereolithography of Three-Dimensional Bioactive Poly(Ethylene Glycol) Constructs with Encapsulated Cells. Ann. Biomed. Eng. **34**(9), 1429, 2006;

109. Grogan SP, Chung PH, Soman P, Chen P, Lotz MK, Chen S, D'Lima DD. Digital micromirror device projection printing system for meniscus tissue engineering. Acta Biomater. **9**(7), 7218, 2013;

110. Lee S-H, Moon JJ, West JL. Three-dimensional micropatterning of bioactive hydrogels via two-photon laser scanning photolithography for guided 3D cell migration. Biomaterials. **29**(20), 2962, 2008;

111. Tsang VL, Chen AA, Cho LM, Jadin KD, Sah RL, DeLong S, West JL, Bhatia SN. Fabrication of 3D hepatic tissues by additive photopatterning of cellular hydrogels. FASEB J. **21**(3), 790, 2007;

112. Bryant SJ, Cuy JL, Hauch KD, Ratner BD. Photo-patterning of porous hydrogels for tissue engineering. Biomaterials. **28**(19), 2978, 2007;

113. Papavasiliou G, Songprawat P, Pérez-Luna V, Hammes E, Morris M, Chiu Y-C, Brey E. Three-Dimensional Patterning of Poly(Ethylene Glycol) Hydrogels Through Surface-Initiated Photopolymerization. Tissue Eng. Part C Methods. **14**(2), 129, 2008;

114. DeForest CA, Polizzotti BD, Anseth KS. Sequential click reactions for synthesizing and patterning three-dimensional cell microenvironments. Nat. Mater. **8**(8), 659, 2009;

115. Kloxin AM, Kasko AM, Salinas CN, Anseth KS. Photodegradable Hydrogels for Dynamic Tuning of Physical and Chemical Properties. Science. **324**(5923), 59, 2009;

116. Hutson CB, Nichol JW, Aubin H, Bae H, Yamanlar S, Al-Haque S, Koshy ST, Khademhosseini A. Synthesis and Characterization of Tunable Poly(Ethylene Glycol): Gelatin Methacrylate Composite Hydrogels. Tissue Eng. Part A. **17**(13–14), 1713, 2011;

117. Lin S, Sangaj N, Razafiarison T, Zhang C, Varghese S. Influence of Physical Properties of Biomaterials on Cellular Behavior. Pharm. Res. **28**(6), 1422, 2011;

118. Fairbanks BD, Schwartz MP, Bowman CN, Anseth KS. Photoinitiated polymerization of PEG-diacrylate with lithium phenyl-2,4,6-trimethylbenzoylphosphinate: polymerization rate and cytocompatibility. Biomaterials. **30**(35), 6702, 2009;

119. Yang X, Sarvestani SK, Moeinzadeh S, He X, Jabbari E. Three-Dimensional-Engineered Matrix to Study Cancer Stem Cells and Tumorsphere Formation: Effect of Matrix Modulus. Tissue Eng. Part A. **19**(5–6), 669, 2012;

120. Marxen M, Sled JG, Yu LX, Paget C, Henkelman RM. Comparing microsphere deposition and flow modeling in 3D vascular trees. Am. J. Physiol. - Heart Circ. Physiol. **291**(5), H2136, 2006;

121. Aung A, Gupta G, Majid G, Varghese S. Osteoarthritic chondrocyte–secreted morphogens induce chondrogenic differentiation of human mesenchymal stem cells. Arthritis Rheum. **63**(1), 148, 2011;

122. Hui EE, Bhatia SN. Micromechanical control of cell–cell interactions. Proc. Natl. Acad. Sci. **104**(14), 5722, 2007;

123. Helmlinger G, Netti PA, Lichtenbeld HC, Melder RJ, Jain RK. Solid stress inhibits the growth of multicellular tumor spheroids. Nat. Biotechnol. **15**(8), 778, 1997;

124. Khavari A, Nydén M, Weitz DA, Ehrlicher AJ. Composite alginate gels for tunable cellular microenvironment mechanics. Sci. Rep. **6**, 30854, 2016;

125. Loessner D, Flegg JA, Byrne HM, Clements JA, Hutmacher DW. Growth of confined cancer spheroids: a combined experimental and mathematical modelling approach. Integr. Biol. **5**(3), 597, 2013;

126. Kaemmerer E, Melchels FPW, Holzapfel BM, Meckel T, Hutmacher DW, Loessner D. Gelatine methacrylamide-based hydrogels: An alternative three-dimensional cancer cell culture system. Acta Biomater. **10**(6), 2551, 2014;

127. Kessenbrock K, Plaks V, Werb Z. Matrix Metalloproteinases: Regulators of the Tumor Microenvironment. Cell. **141**(1), 52, 2010;